RESEARCH ARTICLE

Key Points:

- The pace of arctic sea ice retreat is highly nonlinear
- Loitering occurs over 20–25% of the Seasonal Ice Zone for 4–11 days at a time
- The cause is off-ice winds that force ice floes into warm water where they melt

Correspondence to:
M. Steele,
mas@apl.washington.edu

Loitering of the retreating sea ice edge in the Arctic Seas

Michael Steele[1] and Wendy Ermold[1]

[1]Polar Science Center, Applied Physics Laboratory, University of Washington, Seattle, Washington, USA

Abstract Each year, the arctic sea ice edge retreats from its winter maximum extent through the Seasonal Ice Zone (SIZ) to its summer minimum extent. On some days, this retreat happens at a rapid pace, while on other days, parts of the pan-arctic ice edge hardly move for periods of days up to 1.5 weeks. We term this stationary behavior "ice edge loitering," and identify areas that are more prone to loitering than others. Generally, about 20–25% of the SIZ area experiences loitering, most often only one time at any one location during the retreat season, but sometimes two or more times. The main mechanism controlling loitering is an interaction between surface winds and warm sea surface temperatures in areas from which the ice has already retreated. When retreat happens early enough to allow atmospheric warming of this open water, winds that force ice floes into this water cause melting. Thus, while individual ice floes are moving, the ice edge as a whole appears to loiter. The time scale of loitering is then naturally tied to the synoptic time scale of wind forcing. Perhaps surprisingly, the area of loitering in the arctic seas has not changed over the past 25 years, even as the SIZ area has grown. This is because rapid ice retreat happens most commonly late in the summer, when atmospheric warming of open water is weak. We speculate that loitering may have profound effects on both physical and biological conditions at the ice edge during the retreat season.

1. Introduction

Arctic sea ice extent is on the decline. This generally holds true for all seasons, all months, and all regions, although with some exceptions and with significant interannual variability within multiyear linear trends [*Cavalieri and Parkinson*, 2012]. On a shorter time scale, Figure 1 (upper curves) shows how Northern Hemisphere sea ice extent varies over the year (see section 2, for details on the data set used here). Seasonal ice extent varies not as a pure sinusoid, but rather more like a curtate cycloid [e.g., *Steele et al.*, 2001], with a long winter (December to mid-June, or ~6.5 months above the mean extent line for the most recent period) and shorter summer (mid-June to November, or ~5.5 months below the line). If we assume that extent comprises a perfect circle, then the time derivative of its radius is a simple measure of the average rate of ice retreat (in spring and summer) or advance (in fall and winter). These curves are also plotted in Figure 1. They look very similar to the time derivative of extent (not shown). Unlike for extent, the period of retreat (mid-March to mid-September, or ~6 months) is about equal to the period of advance (mid-September through mid-March).

The ice retreat season starts in March, with a linear increase in the retreat rate through April; i.e., a constant acceleration. This acceleration slows or ceases during May and part of June, a "retreat acceleration (RA) hiatus" that is driven by the geometric constriction of ocean area through the peripheral seas and straits that connect the Arctic Ocean with the North Atlantic and North Pacific Oceans [*Eisenman*, 2010]. After the sea ice edge enters the Arctic Ocean, retreat acceleration resumes until the retreat rate peak in July. Thereafter, the pace of retreat slows until the mid-September extent minimum, at which time a quick ramp-up to rapid advance begins. After October, advance slows through the rest of the growth season, with an "advance deceleration (AD) hiatus" in November forced by coastal geometry just like the RA hiatus. In summary, the pace of ice retreat accelerates through much of the retreat season, while the pace of ice advance decelerates through most of its season.

Figure 1 (red curves) indicates that for the most recent years, the rate of sea ice retreat after the start of the RA hiatus has increased, and that the July retreat rate maximum has expanded to include parts of June and August. Areal mean retreat rates within the Arctic Ocean are now typically >5 km/d except at the very end
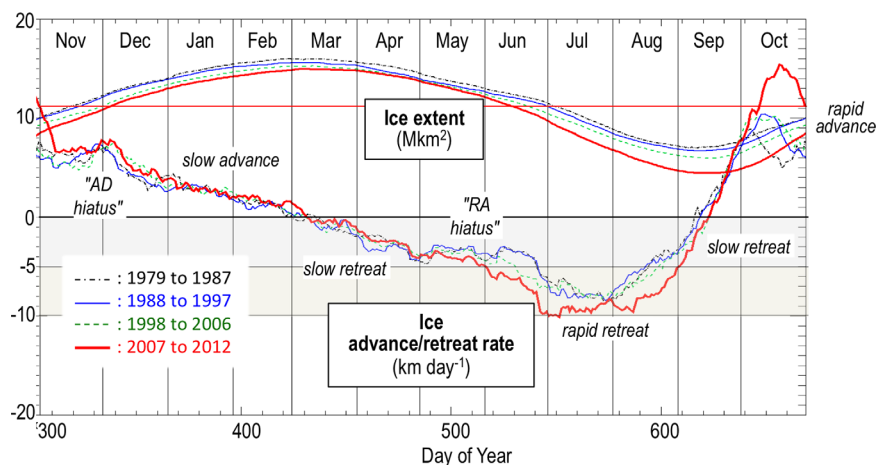
Figure 1. The seasonal variation of Northern Hemisphere sea ice extent (upper curves) averaged into multiyear means, from NSIDC passive microwave satellite concentration (http://nsidc.org/data/nsidc-0051), where extent is defined as the area covered by concentrations ≥15%. Day of Year (horizontal axis) starts in November and runs consecutively through the following October. The horizontal red line is the annual mean ice extent for 2007–2012. Also shown is the rate of ice advance (positive) or retreat (negative), assuming the extent fills a circle and taking the rate of change of its radius. The advance deceleration (AD) hiatus and retreat acceleration (RA) hiatus are explained in the text.

of summer, and the period of most rapid retreat (now ∼9–10 km/d) is nearly 2 months long. (Note that 1 km/d = 1.2 cm/s; e.g., 9–10 km/d = 11–12 cm/s.) Also notable is the large increase in fall rapid advance in recent years, driven by the historically small extent minima that freeze over quickly when the surface energy balance turns negative.

Figure 1 is intriguing, but lacks information about regional differences in retreat rate, which can be substantial [e.g., *Steele et al.*, 2015]. In order to show such regional differences, we present in Figure 2 a new visualization of sea ice retreat (see section 2, for details on the data used). Here we have simply plotted the 15% ice concentration contour (the typical definition of the ice edge and thus the outer boundary for ice extent) for each day of the retreat season, defined here as starting 1 week before the winter maximum extent for each year (i.e., 1 week before the first zero crossing in the lower curves of Figure 1) and ending 1 week after the summer minimum extent (i.e., 1 week after the second zero crossing in Figure 1). Winter maximum and summer minimum dates are provided in Table 1. Three years are shown in the figure: 2011 (a year with moderate ice retreat, relative to recent years), 2012 (the historic maximum ice retreat as of spring 2015), and 2013 (a year with relatively little ice retreat, again relative to recent years). Each day's ice edge is represented by a thin contour line, which generally encloses less area as the summer progresses. The area over which sea ice retreats is referred to here as the Seasonal Ice Zone (SIZ).

There is a lot of information in these simple maps. We focus here on the spacing of edge contours, which indicates the rate of ice retreat. If this rate were constant and nonzero through the retreat season, then these contours would be equally spaced. However, this is clearly not the case. For example, in 2012, we see an area of sparse contours in the center of the western Arctic Ocean SIZ north of Alaska and far eastern Siberia, where the ice edge was retreating rapidly toward its historic minimum of that year. On the other hand, we see other areas where ice edge contours are "overplotting" on top of each other, making apparently darker, thicker contours. For example, two such areas are evident in 2012 in the Beaufort Sea north of Alaska (red box). This overplotting is an indication that ice retreat has slowed considerably over a period of several days or more. We refer to this phenomenon as "ice edge loitering." We could just as well call this "ice edge stalling" or "slowing" or some other word that indicates a reduction in the rate of retreat that leads to a relatively stationary ice edge position over the course of several days or more. Figure 2 indicates that loitering is a pan-arctic phenomenon that occurs each retreat season.

Figure 1 shows that the hemisphere-mean rate of sea ice retreat varies over the spring and summer. Figure 2 further indicates that regionally, the rate of retreat can vary quite dramatically. Given recent interest in the dramatic retreat of the sea ice pack over the past few decades, we are motivated here to study the detailed behavior of retreat on a daily basis. Specifically, the goals of this study are to define, quantify, and explain ice edge loitering in the arctic seas during the retreat season. Our paper is structured as follows: section 2
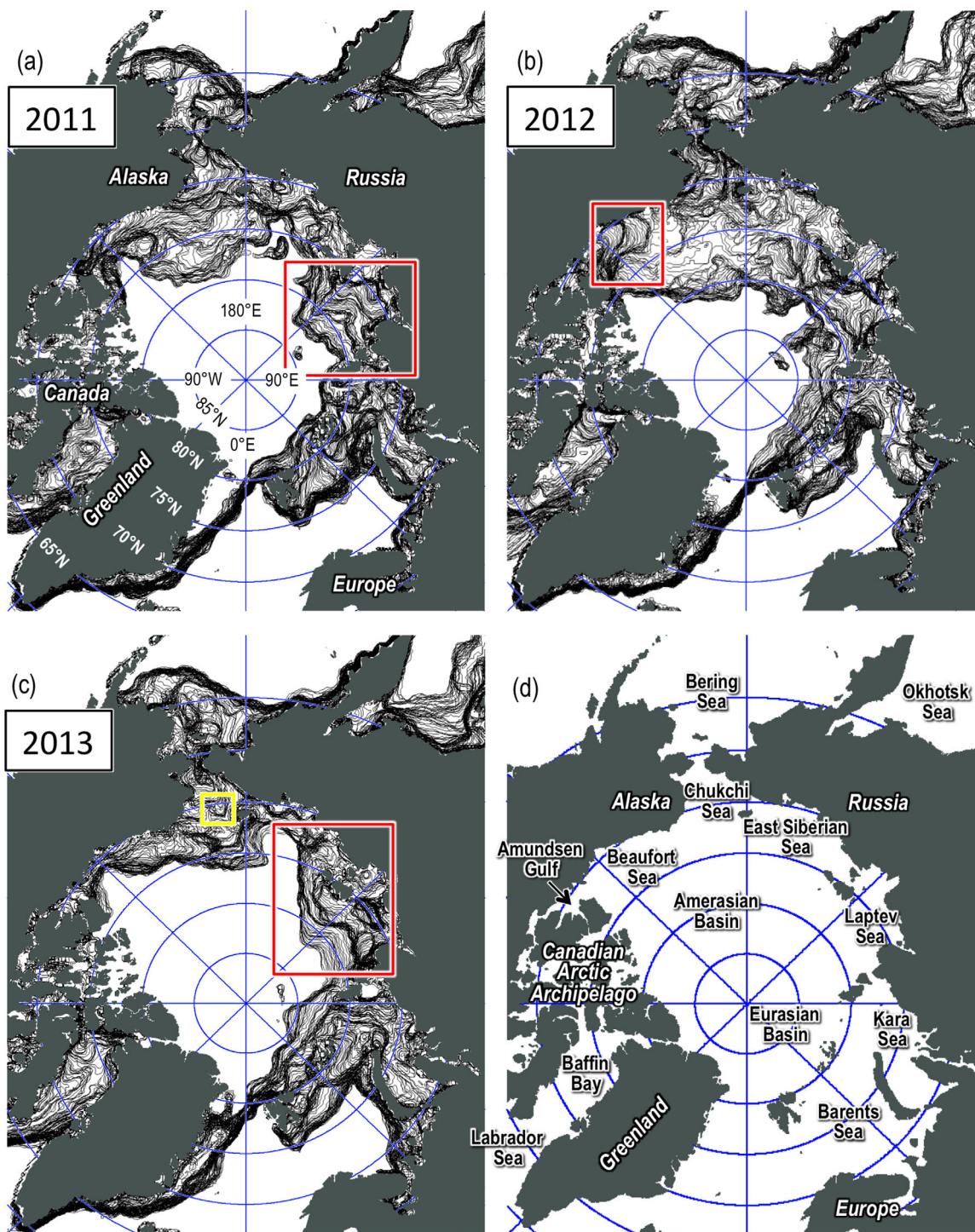
Figure 2. The daily mean ice edge (defined as the 15% ice concentration contour, using the same data as in Figure 1), for each day of the retreat season (see text for retreat season definition). Shown are daily mean ice edges for (a) 2011, (b) 2012, and (c) 2013. (d) Oceanographic place names. Red box in Figure 2a refers to area of focus in section 5.3, red box in Figure 2b refers to analysis in Figure 3, and red box in Figure 2c refers to analysis in Figure 5. Yellow box in Figure 2c refers to possible Taylor column loitering (section 5.1).

presents the data used in this study, while section 3 discusses our methods, including a glossary of terms related to loitering. Section 4 then presents more information about loitering, including a discussion of where and when loitering is more or less likely to occur, and a survey of its variation over previous years. Section 5 provides a physical explanation for loitering, focusing on a series of loitering events found in the Laptev Sea in the summer of 2011. Section 6 provides a summary and discussion.

Table 1. Dates of Maximum (Max) and Minimum (Min) Northern Hemisphere Sea Ice Extent, Using the Same Data as in Figure 1, for the Years 2007–2013[a]

	Max	Min
2007	Mar 12	Sep 18
2008	Mar 13	Sep 20
2009	Mar 5	Sep 13
2010	Apr 2	Sep 21
2011	Mar 9	Sep 11
2012	Mar 20	Sep 16
2013	Mar 15	Sep 13

[a]Mar = March, Apr = April, Sep = September. The ice retreat season for each year is defined here as starting 1 week before the maximum and ending 1 week after the minimum.

2. Data

In this study, we analyze satellite, atmospheric reanalysis, and atmospheric station data concerning sea ice concentration, sea surface temperature, and surface winds. Ice concentration data were obtained from three sources. Our primary data source is a long time series from the National Snow and Ice Data Center (NSIDC) that uses SMMR (1979–1987), SSM/I (1987–2007), and SSMIS (2007–present) passive microwave sensors processed with the NASA Team algorithm, provided at 25 km spatial resolution [*Cavalieri et al.*, 1996]. We here use data from SSM/I and SSMIS, starting in 1989, since these are provided as daily means. Concentration accuracy is provided by NSIDC (quoting) [*Cavalieri et al.*, 1992] as 5% in winter and 15% in summer. We also analyzed sea ice concentration data from the more recently available high-resolution AMSR2 passive microwave sensor, available at 3.125 km resolution from the University of Hamburg [*Beitsch et al.*, 2014]. The accuracy of this algorithm was estimated for the older but similar AMSR-E sensor as ∼25% near the ice edge, linearly improving toward ∼6% in 100% pack ice [*Spreen et al.*, 2008].

We also analyzed ice extent data from NSIDC's Multisensor Analyzed Sea Ice Extent (MASIE) product [*Fetterer et al.*, 2010]. This is a daily 4 km resolution field with each pixel containing "ice" or "no ice" produced by an analyst at the National Ice Center (NIC) from visible and passive microwave satellite data plus weekly NIC analyzed ice charts (which include in situ observations); we used data from 2007 to the present. Overall errors have not been determined, but a similar product for the Canadian Beaufort Sea estimated ice edge position error at 10 km [*Tivy et al.*, 2011]. For comparison with the 25 km resolution passive microwave product, the MASIE data were transformed into an ice concentration field by collecting the 4 km data into two-dimensional running 7 by 7 bins. The impact of ice concentration errors on our results is discussed in sections 3 and 6.

We also analyze sea surface temperature (SST) data using NOAA's OI.v2 data set, a global, daily mean product with 0.25° spatial resolution [*Reynolds et al.*, 2007]. We use the version derived from AVHRR infrared sensors only, which provides a consistent multiyear data set when passive microwave SST is not available. For a previous 1° resolution version of this data set [*Reynolds et al.*, 2002], SSTs were found to be biased relative to in situ observations by ∼0.5°C, with RMS errors up to 1.5°C [*Steele et al.*, 2008].

We also analyze 10 m surface winds from NASA's Modern-Era Retrospective Analysis for Research and Applications (MERRA). This reanalysis provides realistic surface fluxes and winds in the Arctic Ocean relative to independent observations; surface wind speed bias is generally less than 0.4 m/s and correlations $r = 0.7$–0.8 [e.g., *Lindsay et al.*, 2014]. For spectral analysis of wind speed periodicity, we used data from three Laptev Sea coastal stations available from NOAA: Anabar, Cape Terpay-Tumus, and Ust' Olenek over the period 1 June to 11 September for the year 1990 (Anabar and Cape Terpay-Tumus), and the years 2013 and 2014 (Anabar and Ust' Olenek). These are somewhat arbitrary, but they sample both recent and older years. This database provides wind speed to the nearest meter per second (i.e., integer values). Nominal sampling is 3 hourly, but with some gaps that were linearly interpolated. Only some outlier elimination and other initial quality control procedures were performed on these data [*Lott*, 2004].

3. Methods

3.1. Finding the Ice Edge

Following the usual definition [*Parkinson and Cavalieri*, 2008], ice extent is here defined as the area covered by ice concentrations equal to or above 15%. The ice edge is then the outer border of this region. In Figure 2 and section 5, we use a contour-based method to define the ice edge, which provides a smoothed, interpolated view. This is useful for qualitative assessment (as in Figure 2) and for an interpolated estimate of subpixel ice edge displacements (section 5), similar to feature-tracking algorithms used to determine ice pack motion [e.g., *Kwok et al.*, 1998]. For quantitative and statistical analysis of pan-arctic loitering, we also use a pixel-based
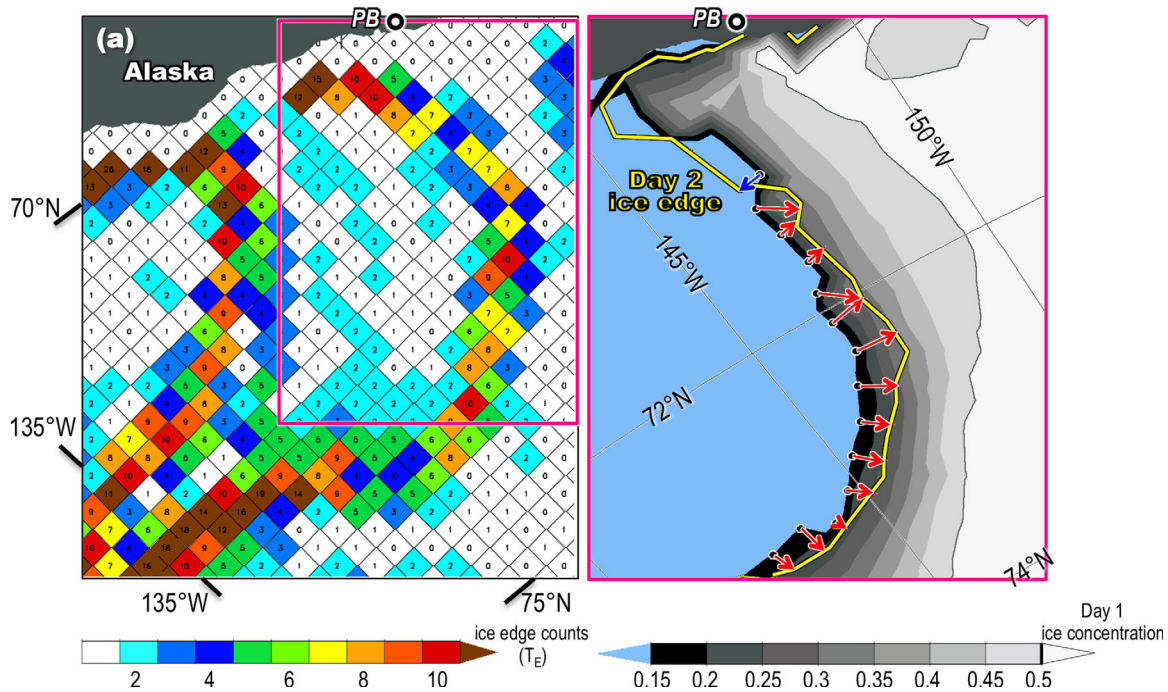
Figure 3. (a) Ice edge counts (T_E) for 25 km resolution pixels in the Beaufort Sea (red box in Figure 2b) during the retreat season of 2012. PB = Point Barrow, Alaska. White pixels denote ice edge counts of 0 or 1. (b) Ice concentration contours (gray shading) on 9 July 2012 (i.e., "Day 1") from a subset of Figure 3a (pink box), showing 25 km resolution along the ice edge (i.e., black dots along the 15% concentration contour). Also shown is the ice edge on 10 July (i.e., "Day 2," yellow line), and vectors pointing in the direction of local "ice north" for retreat (red) and "ice south" for advance (blue). The magnitude of the vectors denotes the ice edge displacement between Days 1 and 2. Displacement is not computed within 100 km of the coast.

method in section 4, since this provides unsmoothed, noninterpolated fields that reflect the input data most accurately. In the first step of the pixel-based method, a field of concentration values at each pixel (e.g., 25 km × 25 km bins for SSMI/SSMIS observations) is converted into a binary field of ones (concentration greater than or equal to 15%) and zeros (lesser values of concentration, including open water). A 3 × 3 two-dimensional running window is then passed over the entire field. For windows with center value equal to one (i.e., ice), the center pixel is within the ice pack if the sum of all nine pixels in the window is equal to nine (i.e., it is surrounded by ice). We here define an ice edge pixel when this sum is less than eight, which implies some open water nearby and which tends to produce ice edges composed of a single row of pixels. A higher sum produces overly thick edges, while a lower sum produces discontinuous edges.

Figure 3a shows how this definition works over the retreat season of 2012 in the Beaufort Sea (red box in Figure 2b). Each pixel shows the number of days T_E that it was designated as an ice edge over the entire retreat season. For example, pixels with $T_E = 0$ were never so designated, while those with a high T_E value were at the ice edge on multiple days (but not necessarily consecutively). The two loitering events noted in Figure 2b are clearly seen in this figure, merging together toward the northeast. Table 2 provides a glossary

Table 2. Loitering Definitions

	Units	Definition
T_E (Total edge time)	days	Total days over a retreat season when a pixel is at the ice edge
T_{n+} (Loiter time)	days	Days in a single loiter event; minimum n = 2
$T_{\Sigma n+}$ (Total loiter time)	days	Total loitering days over a retreat season in a pixel, summed over all loitering events
T_{In+} (Interloiter time)	days	Days between two loitering events in a pixel
N_{n+} (Loiter count)		Number of all loiter events over a retreat season in a pixel
ΣN_{n+} (Artic loiter count)		Sum of all loiter counts N_{n+} in a retreat season over all pixels
N_{In+} (Interloiter count)		Number of all interloiter events over a retreat season in a pixel $N_{n+} = 1$
ΣN_{In+} (Artic interloiter count)		Sum of all interloitering counts N_{n+} in a retreat season over all pixels
F_{n+} (loitering fraction)		Fraction of years over some period with at least one loitering event in a pixel
A_{SIZ} (SIZ area)	km^2	The area over which the ice edge sweeps from winter max extent to summer min
A_{n+} (Loitering area)	km^2	The area over which the ice edge loiters
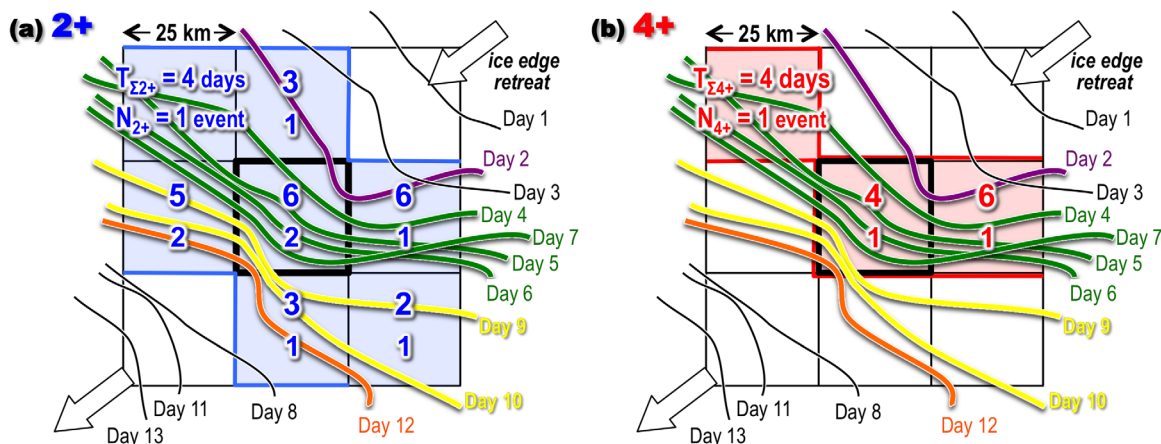
Figure 4. Hypothetical ice retreat over 13 days from top right to bottom left across a 3 × 3 grid of pixels (25 km resolution for SSMI/SSMIS data). The only difference between the two plots is that in Figure 4a, the minimum number of consecutive days needed to define a loitering event is n = 2, while in Figure 4b, this minimum number of days is n = 4. Ice edges are only colored (arbitrarily) if they enter the center pixel (heavy black outline). They retain the same color if they remain in the center pixel on consecutive days. Pixels are shaded if they contain at least one loitering event.

of terms introduced in this paper, including T_E. The area of the SIZ in each year A_{SIZ} is defined as the sum of all pixel areas with concentration greater than 15% at the start of the retreat season that become ice free on any day during the retreat season.

3.2. Ice Edge Coordinates and Displacement

Along each day's ice edge (i.e., the 15% ice concentration contour) with 25 km spacing, we define a local coordinate system wherein "ice north" is directed along the maximum ice concentration gradient, pointing toward higher concentration values. Broadly speaking, the arctic ice edge is roughly zonal, and concentration contours run parallel to the edge, so that "ice north" is generally similar to true north. But of course this is not true for all areas and all times. Figure 3b provides an example for 9 July 2012 in the Beaufort Sea. This is 2 days before the start of the more western of the two loitering events illustrated in Figure 3a. In the northern part of this domain, "ice north" is comparable to true north, but in other areas, "ice north" is in fact pointing more toward the west. Also, small-scale variations in the concentration field can produce somewhat noisy ice edge gradients, which produce "ice north" vectors with some along-edge noise (e.g., at ∼72°N in Figure 3b). Smoothing these vectors along the edge generally changed our estimates of ice edge behavior by less than ∼5–10%, so we chose to forego smoothing. Between 9 and 10 July, the ice edge retreated over much of this domain (red vectors in Figure 3b), although there was some advance in the south (blue vector). Ice edge displacement was not computed within 100 km of the coast, owing to issues with landfast ice (see section 3.3) and possible land contamination of ice concentration data.

3.3. Definition of Loitering

We define a single loitering event as a continuous sequence of n or more days T_{n+} when the ice edge is in a pixel, where n ≥ 2. Each loitering event is delimited by at least 1 day at the start and at the end of the sequence when the ice edge was not in that pixel. For each retreat season, a pixel may contain N_{n+} loitering events, separated by $N_{In+} = N_{n+} - 1$ "interloitering" events. Each interloitering event lasts T_{In+} days. At each pixel, the total number of loitering days in a retreat season (summed over all events) is $T_{\Sigma n+}$. The glossary in Table 2 provides these definitions and others used in this paper.

So what should we use for the loitering parameter n? Figure 4 illustrates two possible options n = 2 and n = 4 for a hypothetical case where the ice is retreating across a 3 × 3 pixel array over the course of 13 days. The ice edge here is generally moving from the top right to the bottom left, but its pace varies daily and retreat reversals (i.e., advances) are possible. A "weak" definition with n = 2 produces a relatively wide area of loitering, with long total loitering times $T_{\Sigma 2+}$ and multiple events N_{2+}. On the other hand, a more "strict" definition with n = 4 produces a relatively narrow loitering area, with some shorter total loitering times $T_{\Sigma 4+}$ and fewer events N_{4+}.
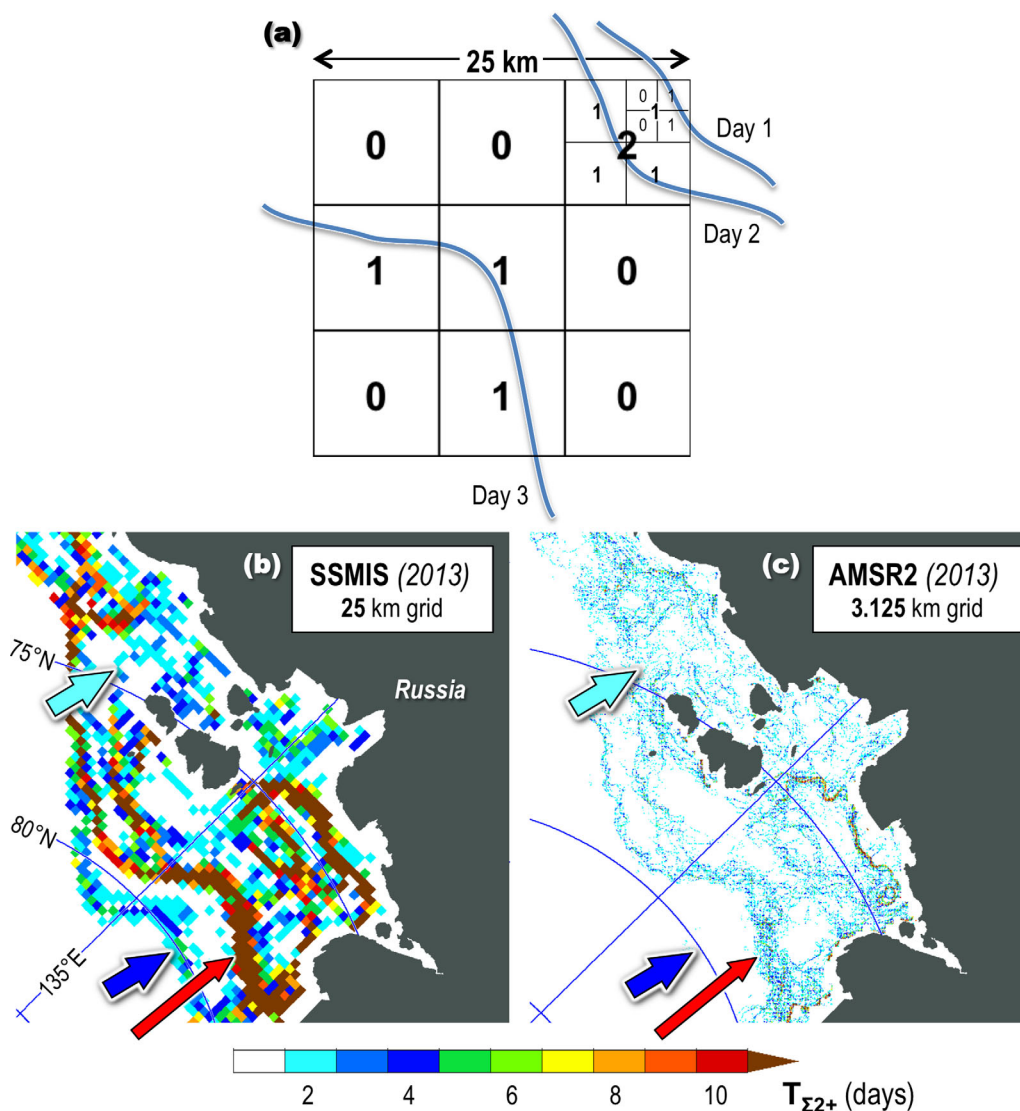
Figure 5. (a) Hypothetical sea ice retreat across a 25 km × 25 km pixel from top right toward bottom left, with T_E noted in each subpixel, and increasing spatial grid resolution in the top right. (b) Total loitering days for n = 2 ($T_{\Sigma 2+}$) for the Laptev and western East Siberian Seas (red box in Figure 2c) when using SSMIS data at 25 km resolution. (c) Same as Figure 5b, but when using AMSR2 data at 3.125 km resolution. Red, dark blue, and light blue arrows mark loitering areas (described in text).

The actual ice edge likely moves at a variable speed, which generally produces loitering at subpixel spatial scales. This is illustrated in Figure 5a for a hypothetical area where the ice edge is moving from top right toward bottom left. If this entire region was one 25 km × 25 km pixel, then $T_E = T_{\Sigma 2+} = 3$ days, i.e., for n = 2, we would designate this as a loitering pixel with one event, i.e., $N_{2+} = 1$. Now imagine that we have another source of data for this time and location with 3 times the resolution, giving us nine pixels. In this case, eight of the pixels would have $T_E = 0$ or 1 days, i.e., no loitering. However, the upper right pixel contains a slow-moving ice edge that is still loitering at this finer scale. In this new upper right pixel, $T_E = T_{\Sigma 2+} = 2$ days and $N_{2+} = 1$. But now imagine that in this upper right pixel, we have yet another source of data with twice the resolution, giving us $T_E = 1$ days, $T_{\Sigma 2+} = 0$ days, and $N_{2+} = 0$ in all four pixels, i.e., no loitering at this spatial scale. In the limit it is unlikely to find loitering for infinite resolution. Thus, loitering depends on the spatial scale of our input data. It also depends on the time scale, but here we only consider data sets with daily mean resolution.

An example using real observations is provided in Figures 5b and 5c, where we compare SSMIS and AMSR2 total loitering days $T_{\Sigma 2+}$ from the Laptev and western East Siberian Seas in 2013. The lower-resolution

SSMIS data generally produce longer total loitering times over a larger area (e.g., compare the loitering area noted by the thin red arrow in Figures 5b and 5c). With regard to subpixel loitering, we compare the two areas denoted by the dark blue and light blue arrows in Figures 5b and 5c. The dark blue arrow marks an area where relatively short period ($\leq$3 days) loitering occurs at low resolution (Figure 5b), but is not apparent in the higher-resolution data (Figure 5c). This could result from a rapid, generally constant ice edge movement across the 25 km pixels. On the other hand, the light blue arrow marks an area where short-period loitering occurs in both the low and high-resolution data. This could result from variable-speed translation of the ice edge, which produces loitering on smaller scales (as in the upper right corner of Figure 5a).

We desire a loitering definition for an ice edge moving slower than average in some sense. Figure 1 indicates that for much of the retreat season in recent years (red curves) hemisphere-mean ice retreat rates are 4–10 km/d (=5–12 cm s^{-1}). Alternatively, we can also consider average sea ice floe speeds within the pack, as diagnosed from drifting buoy displacements and satellite feature-tracking algorithms in the arctic seas. An analysis of such observations for the years 1979–2001 found summer speeds generally less than or equal to $\sim$5 cm s^{-1} [*Martin and Gerdes*, 2007]. However, more recent studies indicate a rapid acceleration of arctic sea ice floes [*Rampal et al.*, 2009] to values closer to $\sim$12 cm s^{-1} at the end of summer [*Spreen et al.*, 2011] or 8 km/d in winter [*Olason and Notz*, 2014].

How long does it take an ice edge moving during summer at a constant speed of 12 cm s^{-1} = 10 km/d^{-1} to cross a 25 km square pixel? The mean caliper diameter [e.g., *Rothrock and Thorndike*, 1984] is the distance across the square, averaged over all angles = 4 × 25 km/π = 32 km. Thus, the ice edge takes 32 km/10 km/d = 3.2 days to cross the pixel. Loitering then requires a value for n that is higher than this mean value of 3 days.

Figure 6 shows pan-arctic loitering maps of total loitering time $T_{\Sigma n+}$ for the retreat seasons of 2011–2013, for two possible choices n = 2 and n = 4. Loitering by either definition is seen in each year. As just discussed, a loitering definition of $T_{\Sigma 4+}$ guarantees a slower-than-average ice retreat speed. The bottom row of Figure 6 indicates that this choice nicely highlights the main loitering features seen in the top row and in Figure 2. We also considered a longer-period loitering definition $T_{\Sigma 6+}$, but this resulted in drastically fewer loitering areas than Figure 2 suggests. Note that maps of $T_{\Sigma 4+}$ cannot be derived from maps of $T_{\Sigma 2+}$ simply by eliminating pixels where $T_{\Sigma 2+} < 4$ days; a second step is necessary to then eliminate pixels with $T_{\Sigma 2+} \geq 4$ days but $N_{4+} = 0$ (i.e., pixels with multiple short-period loitering events, e.g., the left center pixel in Figure 4).

In summary, we propose a somewhat strict loitering definition wherein the ice edge must remain in a 25 km pixel for a minimum of 4 days, thus focusing on longer-lasting loitering events. This defines a speed threshold of 32 km (i.e., the mean caliper diameter)/4 days = 8 km/d; ice edges traveling slower than this are designated as loitering. In the following section, we explore where, when, and how long loitering occurs. We also consider interannual variability and trends in arctic loitering.

4. Pan-Arctic Loitering: Spatial and Temporal Extent and Interannual Variability

In this section, we quantify loitering in both space and time, and explore how it has changed since the late 1980s. We use 25 km SSMI/SSMIS data with the n = 4 definition of loitering, which in the previous section (see especially Figure 6), we found best captures the phenomenon. Reference is also made to results using other values for n.

Where does loitering tend to happen year after year? This is partly addressed by Figures 2 and 6, which show loitering in three recent years. An analysis for 1989–2013 (Figure 7a) shows, for each pixel, the fraction of years F_{4+} over the 25 year period when at least one loitering event occurred during the retreat season, i.e., F_{4+} = sum[min(1,N_{4+})]/25 years, where "sum" refers to the summation over all years. The East Greenland Current winter maximum loiters strongly in each year, with little variation in position, and so has the highest amplitude in the figure. Other winter maxima experience more interannual variability in their position, and so have lower amplitude in Figure 7a (especially in the Bering Sea). Within the eastern Arctic Ocean SIZ, the northern sectors of the Barents, Kara, and Laptev Seas show a high tendency to loiter. For the western Arctic Ocean SIZ, loitering is most frequent in the eastern and central Beaufort Sea, the northern Chukchi Sea, and far northern Baffin Bay. Amplitudes in these "loitering-prone" areas are reduced relative to the strongest winter extent maxima, owing to interannual variability. That is, these areas tend to experience loitering in most years, but not necessarily in the exact same locations. This is also why loitering
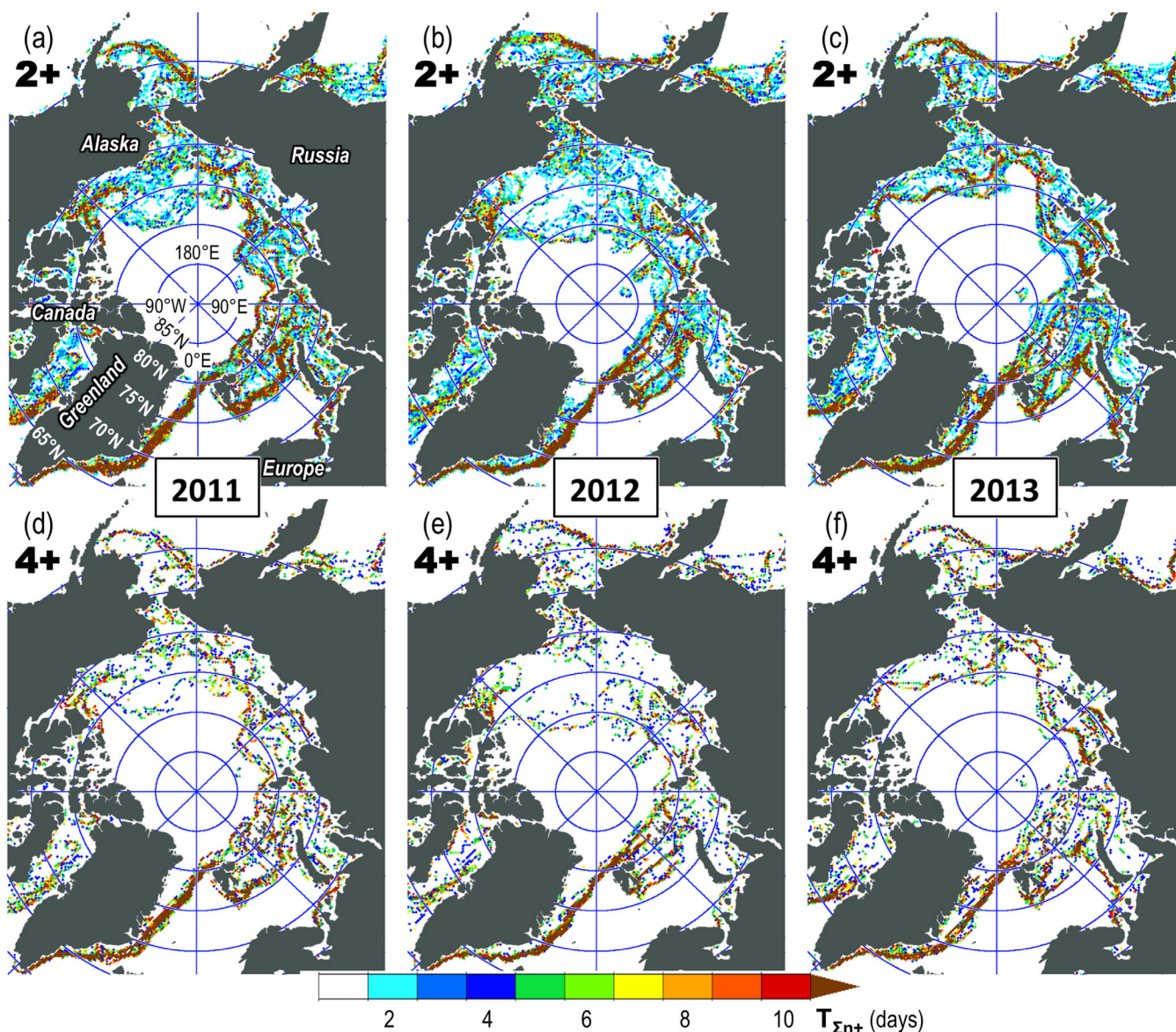
Figure 6. Pan-arctic maps of the total number of days loitered $T_{\Sigma n+}$ for the retreat seasons of 2011–2013, using two values of n: (top) n = 2 (i.e., "2+") and (bottom) n = 4 (i.e., "4+"). Ice concentration is from SSMIS data.

at the summer extent minimum, evident in Figures 2 and 6, hardly appears in Figure 7a. Finally, note that some areas within the SIZ experience less frequent loitering, notably the East Siberian Sea, the western Beaufort Sea, the Northeast Greenland shelf, the southern Chukchi and northern Bering Seas, and most southern Russian arctic shelves.

Enhanced loitering is observed seaward of landfast ice, e.g., west of Amundsen Gulf in the eastern Beaufort Sea and north of the shallowest part of the Laptev Sea shelf. However, this is not true loitering, but rather a consequence of how the ice concentration data set treats the mobile sea ice pack and the (mostly) immobile landfast ice zone in the same way. That is, as the pack ice retreats away from the landfast ice (generally in May and June), the outer boundary of the latter is marked in the ice concentration field as a stationary transition from 100% to 0% ice, which remains in place (i.e., "loiters") until the landfast ice breaks up after several weeks.

For comparison, an analysis using the MASIE data set is shown in Figure 7b. The general pattern of loitering-prone and loitering-free areas is similar in the two plots of Figure 7. However, loitering amplitudes are consistently higher in MASIE relative to SSMIS for reasons that are not clear to us at this time.
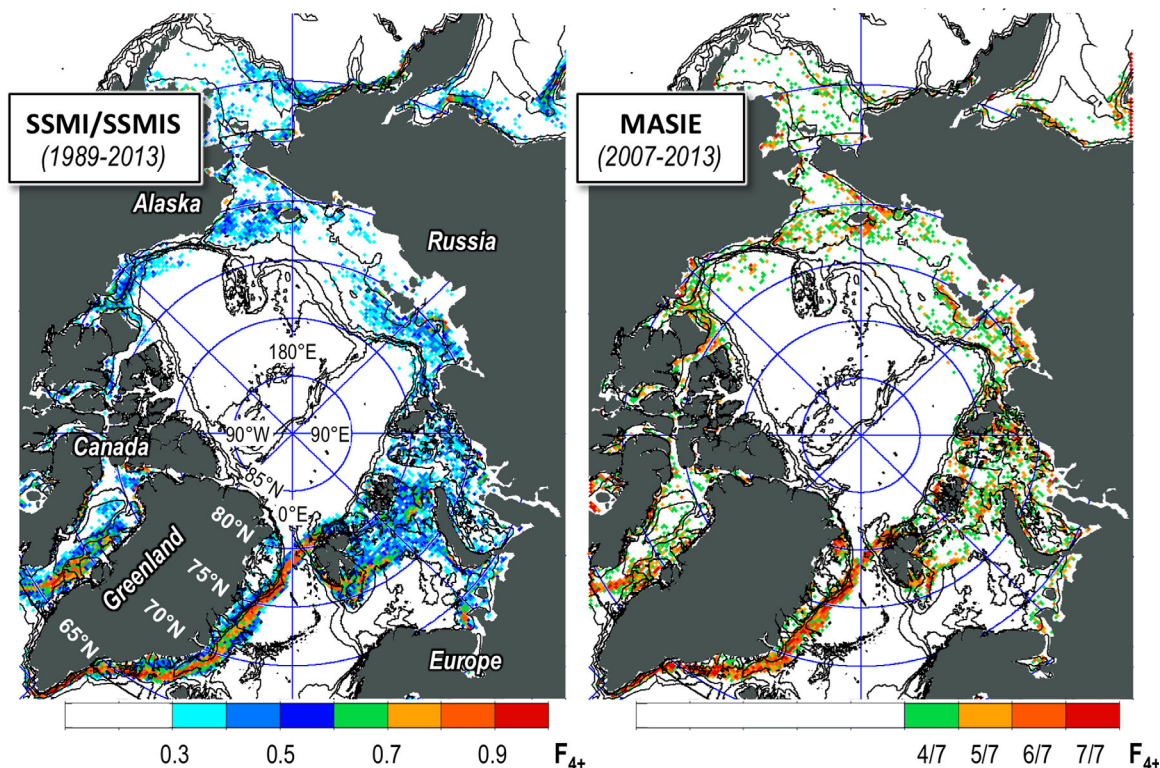
Figure 7. Loitering frequency F_{4+} for (a) SSMI/SSMIS and (b) MASIE. Each pixel shows the fraction of years over the time period indicated that at least one loitering event occurred (for n = 4 days). Color scales emphasize areas with persistent loitering; MASIE has higher values everywhere, relative to SSMI/SSMIS. Isobaths are plotted for depths of 30, 100, 300, 1000, and 2000 m.

Figure 8 presents quantitative loitering statistics for the 2011 retreat season, a moderate (by today's standards) ice retreat year. Comparison with other years is provided in Figure 9. The analysis shown here is for the entire Northern Hemisphere sea ice pack, i.e., extending southward outside of the domain presented in Figures 2 and 6. Our first question is how much of the SIZ loitered in 2011? Figure 8a indicates that $A_{4+} = 23\%$, i.e., about a quarter of the SIZ area $A_{SIZ} = 10.7$ Mkm^2 loitered in this year, amounting to 0.23×10.7 Mkm^2 = 2.46 Mkm^2 of loitering area. Figure 8a also shows that total loitering $T_{\Sigma 4+}$ was longer than 11 days for only about 4% of the SIZ. Thus, (23%–4%)/23% = 83% of loitering pixels loiter for $T_{\Sigma 4+} = 4$–11 days. The percent of the SIZ that loiters changes by only ∼2% if we discount areas near the winter extent maxima. However, the number is sensitive to our choice of n: for the 2011 retreat season, $A_{2+}/A_{SIZ} = 50\%$, while $A_{6+}/A_{SIZ} = 10\%$ (not shown).

Total loitering $T_{\Sigma 4+}$ is the sum over a retreat season of all loitering days for all events in a pixel. So how many events are there in a pixel? Figure 8b shows that about 3/4 of loitering pixels (73%) experience only one loitering event, with 96% having up to three events. How long does each loitering event last? This is shown in Figure 8c, which differs from Figure 8a in that here we examine the duration of individual events T_{4+}, rather than the retreat season sum $T_{\Sigma 4+}$. The figure shows that 80% of loitering events last 4–7 days, while 94% last up to 11 days. Finally, Figure 8d shows how many days lie between loitering events. About half of multiple loitering events are separated by six or fewer days. However, there are many events separated by several weeks or more, as large-scale shifting of the pack (likely wind driven) brings the ice back to a pixel that has been ice-free for many days [e.g., *Steele et al.*, 2015, Figure 2].

What are the long-term trends and interannual variability in loitering statistics presented in Figure 8? The area of the SIZ A_{SIZ} has expanded since 1989 by over 1 Mkm^2 (Figure 9a), at least partly in response to the large decline in summer minimum ice extent. At the same time, the area of loitering A_{4+} has generally varied between 2.4 and 3.0 Mkm^2, but with no significant long-term trend. This means that the percent area of the SIZ that loiters $100 \times A_{4+}/A_{SIZ}$ has slowly declined over the past 25 years, from ∼25% to ∼21%. What is the physical explanation for this behavior? The answer is that expansion of the SIZ has involved rapid ice
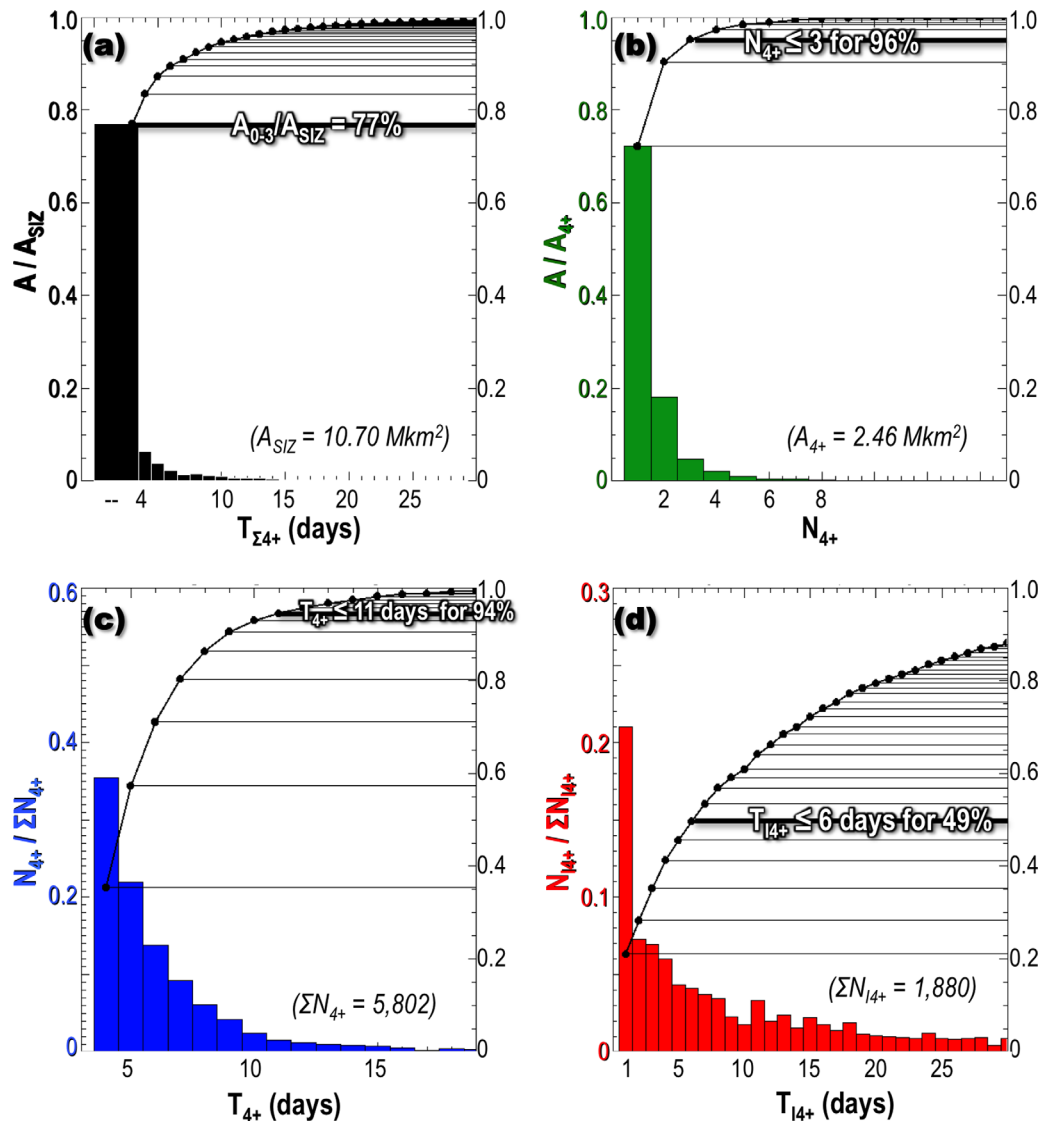
Figure 8. Summary loitering statistics for the retreat season of 2011, i.e., (a) total loitering time $T_{\Sigma 4+}$, (b) number of loitering events N_{4+}, (c) loitering time in each event T_{4+}, and (d) number of days between loitering events T_{I4+}. Left scales refer to the histogram bars, and right scales refer to the cumulative curves. Histogram colors correspond to multiyear analyses presented in Figure 9.

retreat that does not in general involve much loitering. A good example is the historically extreme sea ice retreat year of 2012, marked in Figure 9a, when A_{SIZ} was extreme but A_{4+} was not. Figures 2 and 6 show that in this year, loitering-free areas formed in the northern part of the SIZ in the Amerasian Basin, toward the end of the retreat season. The reason for this will be discussed in section 5.5. We also analyzed trends in loitering area using the MASIE ice data, and found similar results (although over a shorter time period 2007–2013), but with generally higher values relative to those derived using SSMI/SSMIS.

Figure 9b shows interannual time series corresponding to other statistics provided in Figure 8. The fraction of loitering area A/A_{4+} that has only one loitering event $N_{4+} = 1$ (lower green curve) has grown over the past 25 years, while the fraction with three or fewer events (upper green curve) has not. This implies that in earlier years, more pixels had two or three loitering events during each retreat season, while in recent years there has been a shift toward fewer events. The fraction of loitering events $N_{4+}/\Sigma N_{4+}$ that last 4–7 days $T_{4+} \leq 7$ days (lower blue curve) has slightly declined, as has (to a lesser extent) the fraction that last 4–11 days (upper blue curve). This indicates a slight shift to longer-lasting loitering events. Finally, the fraction of interloitering events $N_{I4+}/\Sigma N_{I4+}$ that last 6 days or fewer $T_{I4+} \leq 6$ days has grown, meaning that the time between loitering events is getting shorter.
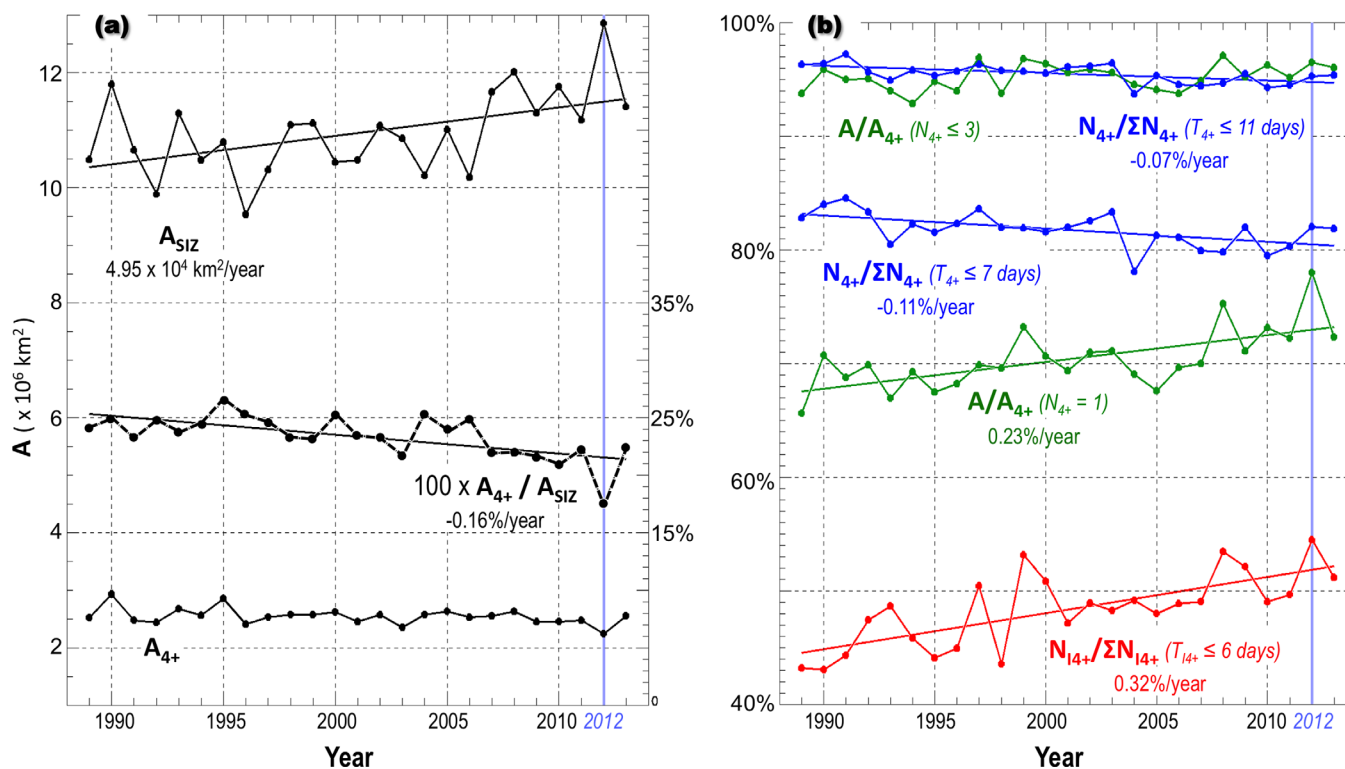
Figure 9. (a) The area A_{SIZ} of the Northern Hemisphere SIZ (top curve, left axis) over the period 1989–2013, which is expanding at a rate of ~50,000 km²/yr. Also shown are the area of loitering A_{4+} (bottom curve, left axis), and the part of the SIZ that is loitering each year A_{4+}/A_{SIZ} (expressed as a percent, dashed middle curve, right axis). The latter is declining at a rate of -0.16% yr^{-1}. Linear trends are shown if they exceed 95% significance. The extreme sea ice retreat year of 2012 is noted with a light blue line. (b) Similar time series corresponding to quantities in Figures 8b–8d (see text for further details).

In summary, loitering (defined with n = 4 days using 25 km passive microwave ice concentration data) covers about 2.5 Mkm² every year, and about 20–25% of the SIZ, although this percent is declining as the SIZ area is expanding (Figure 9a). Loitering tends to happen in some places more than others (Figure 7), with a typical duration of several days and up to 1.5 weeks (Figures 8 and 9b). Most often, loitering happens only once at a particular location during the retreat season, but multiple loitering events do occur (Figure 8). These multiple events can be separated by just a few days or by several weeks (Figure 8). In recent years, with stronger overall retreat (Figure 1), the trend is toward loitering that happens only once or twice at a particular location, and when it happens more than once, the time period between events is shrinking (Figure 9a). One might picture this as an ice edge that used to loiter, then retreated for a while, then returned and loitered again; i.e., an ice edge that was not in a hurry to move northward. In recent years, however, the ice edge has tended to retreat more monotonically northward, while still loitering in the same general areas as in earlier years (but not multiple times).

5. Physical Influences on Loitering: The Interplay Between Wind and Ocean Temperatures

In this section, we explore the mechanisms that produce loitering. We first discuss the roles of bathymetry and variable ice thickness. We then focus on loitering in the Laptev Sea to illustrate the dominant forcing within the SIZ, which involves a interplay between surface winds, sea surface temperature, and the sea ice pack. These ideas are then used to discuss loitering on pan-arctic scales and from a simple theoretical heat flux calculation.

5.1. The Role of Bathymetry

The position of the winter sea ice extent maximum (where loitering is the norm) is often tied to the presence of ocean thermal fronts that are constrained at least partly by bathymetry, i.e., by a transition from shallow shelf to deep basin [Nghiem et al., 2012]. Examples are the shelf breaks of the East Greenland and

Bering Seas, and bathymetric features of the northern Labrador and northern Barents Seas. The physical mechanism operating here involves an interaction between atmospheric surface winds and warm ocean currents. At these bathymetric features, warm ocean currents are moving poleward or are recirculating along the shelf break. In winter, the ice pack has expanded southward toward these warm currents, at which point further expansion is limited by melting. That is, if winds blow the ice pack into this warm water, ice floes will melt and the pack does not advance.

Special bathymetric features might enhance loitering, such as over Herald Shoal in the shallow Chukchi Sea, where a Taylor column traps cold water and inhibits melt [*Martin and Drucker*, 1997]. Enhanced loitering in this area is difficult to detect in Figure 2 or Figure 6, although a weak loitering loop might be evident in Figure 2c (yellow box). A caveat is that our 25 km resolution SSMIS data may not be adequate to resolve this small-scale feature. In fact, Figure 7 indicates that most perennial loitering within the SIZ (i.e., to the north of the winter extent maximum) occurs over the shallow shelves. That is, some (but not all) shelves have loitering ice edges year after year. The reason that some shelves tend to loiter and others do not will be discussed in section 5.5. On the other hand, Figures 2 and 6 clearly show that in any given year, substantial areas of loitering occur over the deep basins as well, although the exact location of these loitering events changes from year-to-year, so that they do not appear in the long-term mean shown in Figure 7. In summary, bathymetry plays some role in loitering via oceanic thermal fronts and circulation, although loitering also occurs in areas where ocean depth variation is relatively small.

5.2. The Role of Ice Thickness
One might imagine that under constant thermodynamic forcing, the retreating ice edge could loiter if it were to encounter a front in ice thickness, where thicker ice would take longer to melt. How can we test this hypothesis? Pan-arctic maps of sea ice thickness have recently become available [*Laxon et al.*, 2013], but only as monthly means. This time scale is unfortunately too long for our purposes. Nonetheless, these data suggest that in recent years, large-scale thickness gradients within or near the SIZ are generally quite weak, except in the eastern Beaufort Sea and northeast of Greenland. This thickness gradient probably controls the summer ice extent minimum in the eastern Beaufort Sea, but it is not clear how it affects loitering within the SIZ itself. Alternatively, daily ice thickness information is available from an observations-assimilating model [e.g., *Schweiger et al.*, 2011], although likely with some unrealistic smoothing owing to various effects, e.g., numerical diffusion and a lack of small-scale atmospheric forcing. Thus, ice thickness variation is unlikely to play a major role in loitering in much of the arctic, but further work on this subject using high-resolution satellite and/or modeling tools could be useful.

5.3. Wind and SST: The Laptev Sea Case Study
In this subsection, we describe an interaction between surface wind, sea surface temperature, and the sea ice pack that our analysis indicates plays a large role in SIZ loitering. To do this, we consider a case study: The Laptev Sea during the 2011 retreat season, which we then broaden to include a number of recent years in this area. Unless noted otherwise, all wind directions described in the rest of the manuscript are in "ice north" coordinates (section 3.2).

The Laptev Sea is a site of perennial loitering (Figure 7); Figures 10a and 10b show how, in 2011, ice retreat was composed of a regular series of loitering events separated by northward ice retreat. Figures 10c and 10d indicate that ice loss was minimal until June, when retreat started to the north of the landfast ice zone that typically resides along the coast in very shallow water [*Eicken et al.*, 2005]. This created an open water area between the landfast ice to the south, the retreating pack ice to the north, and the coasts of the Taymyr Peninsula to the west and the New Siberian Islands to the east. Loitering occurred in late June along the northern edge of this open water area, and also (artificially) along the northern edge of the landfast ice zone (see section 4). By the end of the month, the ocean surface warmed to just over 4°C (Figure 10e). During July 2011 (Figure 10e), the landfast ice broke up, while the pack ice retreated farther north, loitering along two contours that in some places merged into one. Sea surface temperatures continued to warm during this month (Figure 10f). During August and early September 2011 (Figure 10f), more loitering occurred, again primarily along two contours that in some locations merged together. While still well above freezing, the ocean surface began to cool during this time (not shown here; see Figure 13), owing to the late summer decline in shortwave atmospheric fluxes [*Steele et al.*, 2010]. Surface winds were generally easterly along the ice edge in June and July, although this turned around in August and September.
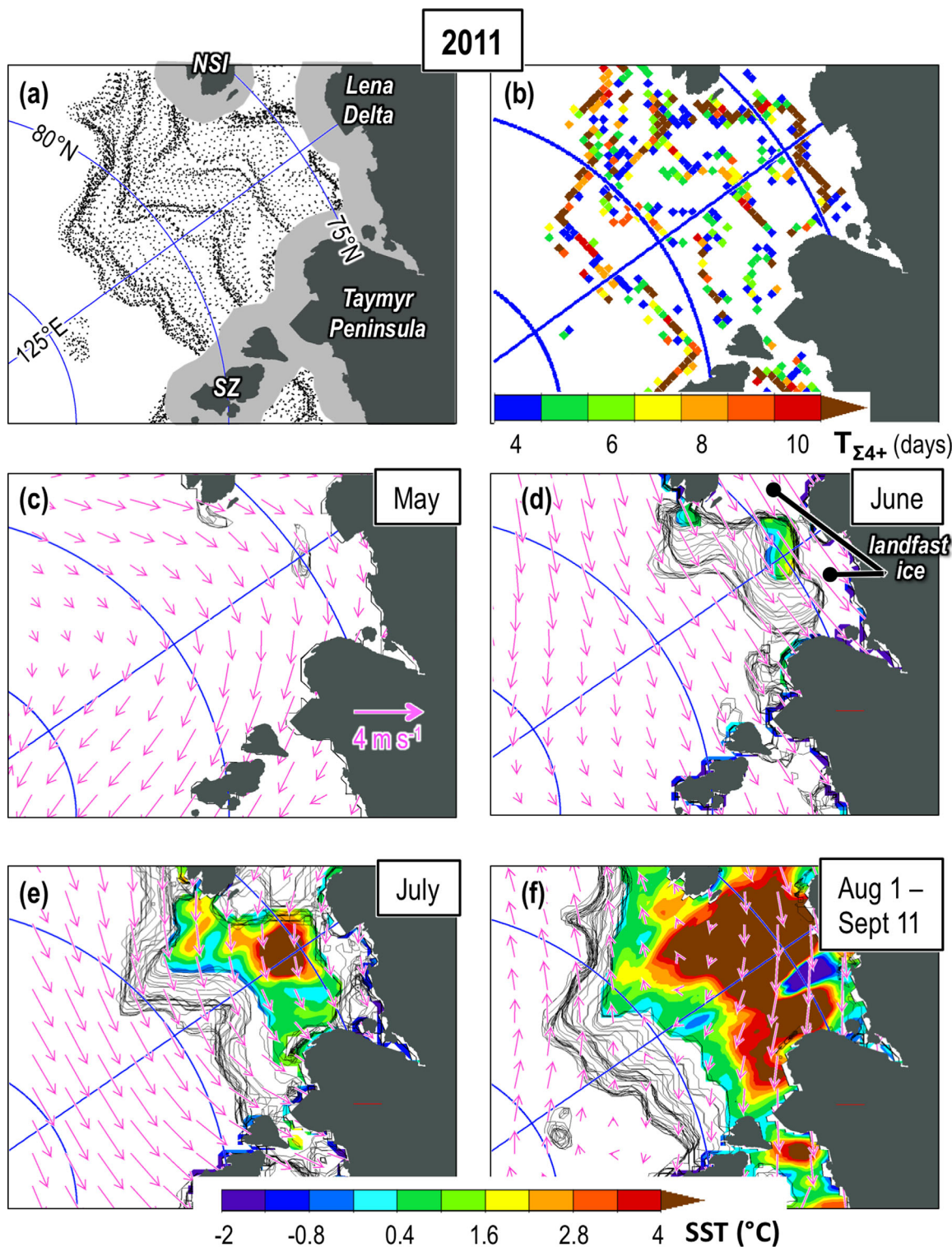
Figure 10. Ice retreat in the Laptev Sea in 2011 (see red box in Figure 2a). (a) Loitering contours showing 25 km resolution ice edge coordinates and 100 km coastal mask (gray shading; see section 3.2); NSI = New Siberian Islands, SZ = Severnya Zemlya. (b) Total loitering $T_{\Sigma 4+}$. (c–f) Four periods during the ice retreat, showing loitering contours (black lines), sea surface temperature at the start of each period (color-filled contours), and vector-mean surface winds (pink arrows; key in Figure 10c).

Over the 2011 retreat season, daily mean surface wind speeds in the Laptev Sea along the ice edge ranged (Figure 11a) from 0 to ∼12 m s^{-1}, with a mode of 4–5 m s^{-1} and a mean of 5.6 m s^{-1}, values similar to pan-arctic summer observations [*Spreen et al.*, 2011]. Wind directions with respect to the ice edge were biased
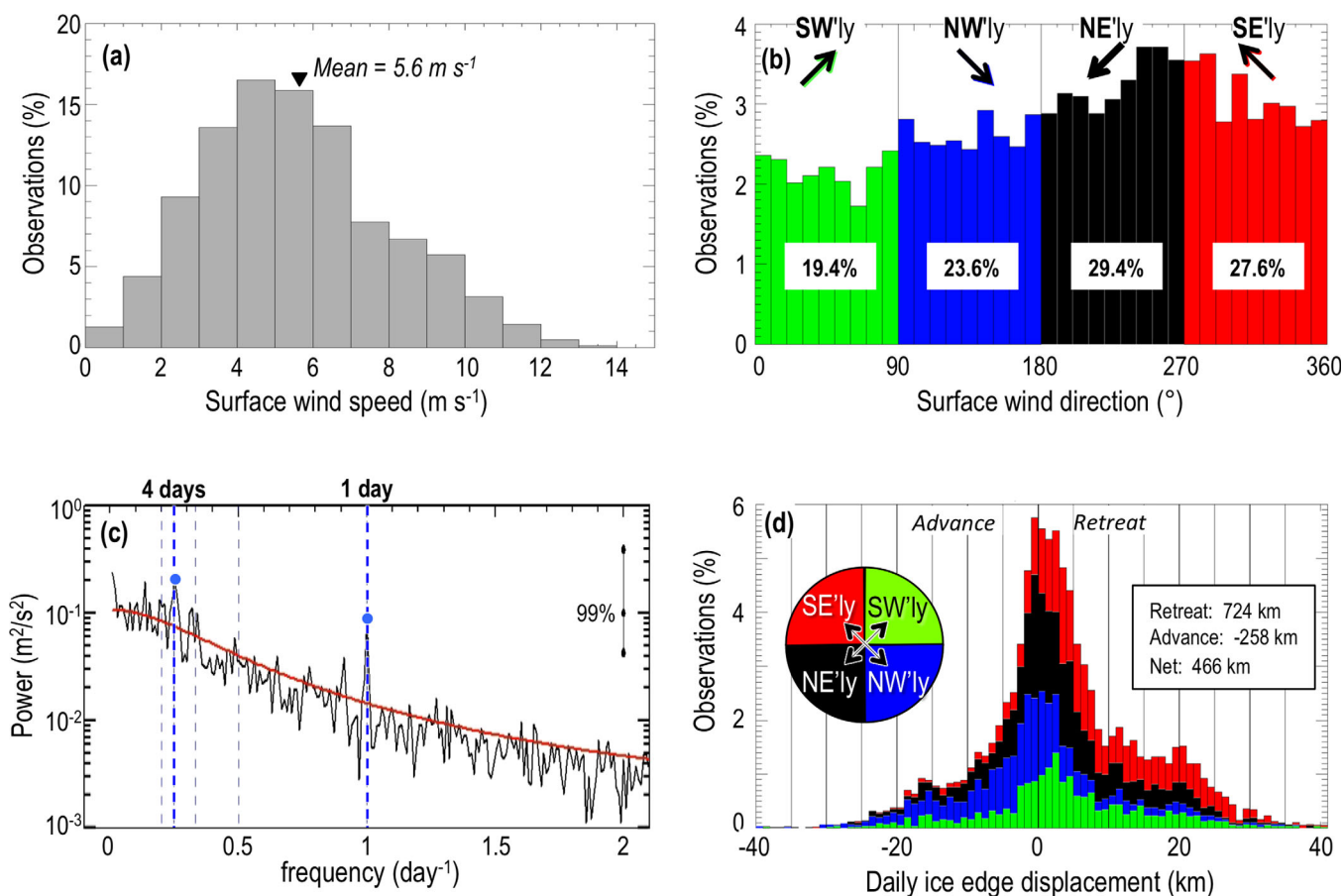
Figure 11. Surface wind statistics in the Laptev Sea (Figure 10 shows domain). (a) Daily mean surface wind speed along the ice edge during the 2011 retreat season. (b) Surface wind direction during the 2011 retreat season, in "ice north" coordinates (section 3.2), colored by four quadrants: southwesterly (SW'ly), northwesterly (NW'ly), northeasterly (NE'ly), and southeasterly (SE'ly). (c) Averaged power spectrum of wind speed (black) for several coastal stations (see text), relative to a red noise model (red), with 1–5 day periods and 99% significant peaks marked (blue dashed lines and blue dots, respectively). (d) Daily mean ice edge retreat (positive displacement) or advance (negative displacement), partitioned by wind direction in ice coordinates along the daily ice edge for the 2011 retreat season.

slightly easterly (Figure 11b), which (see Figure 13) tends to force retreat. (A multiyear average over 2007–2013, not shown, gives nearly identical ice edge wind speeds, and ice edge wind directions that are more uniform with respect to angle.) The time scale of daily mean wind forcing averaged over six historical Laptev Sea coastal meteorological stations (see section 2) has a statistically significant (relative to a simple AR1 red noise model) peak at 4 days (Figure 11c), which is in keeping with classic synoptic wind speed analysis [*van der Hoven*, 1957], and is within the broad synoptic peak derived from older, central Arctic Ocean data [*Lindsay*, 1998]. This time scale is of the same order as the loitering time scales shown in Figure 8c, suggesting that the synoptic variation of surface wind forcing from passing high and low-pressure systems has a key role to play in the loitering process, a topic discussed in further detail below.

Overall ice edge displacement for the area shown in Figure 10 was composed of 724 km of retreat and 258 km of advance; i.e., a net retreat of 466 km (Figure 11d). (Net retreat was greater (~750 km) in the central part of the Laptev north of the landfast ice, but less on the east and west flanks, and much slower along the landfast ice in the early season.) Most daily mean ice edge displacements fell within a range of ±20 km, with fewer values up to ±40 km. Figure 11d also shows that ice retreat was associated more with winds from three out of the four quadrants, especially southeasterly when retreat is strongest. Only northwesterly winds were predominantly (but not exclusively) associated with ice advance. Loitering (defined in section 3 by an absolute ice edge displacement less than 8 km/d) happened 59% of the time in this loitering-prone region, making up 63% (56%) of all advances (retreats). In the following figures, we look in further detail at the relationship between ice edge displacement and retreat or advance. In these analyses, we mark when
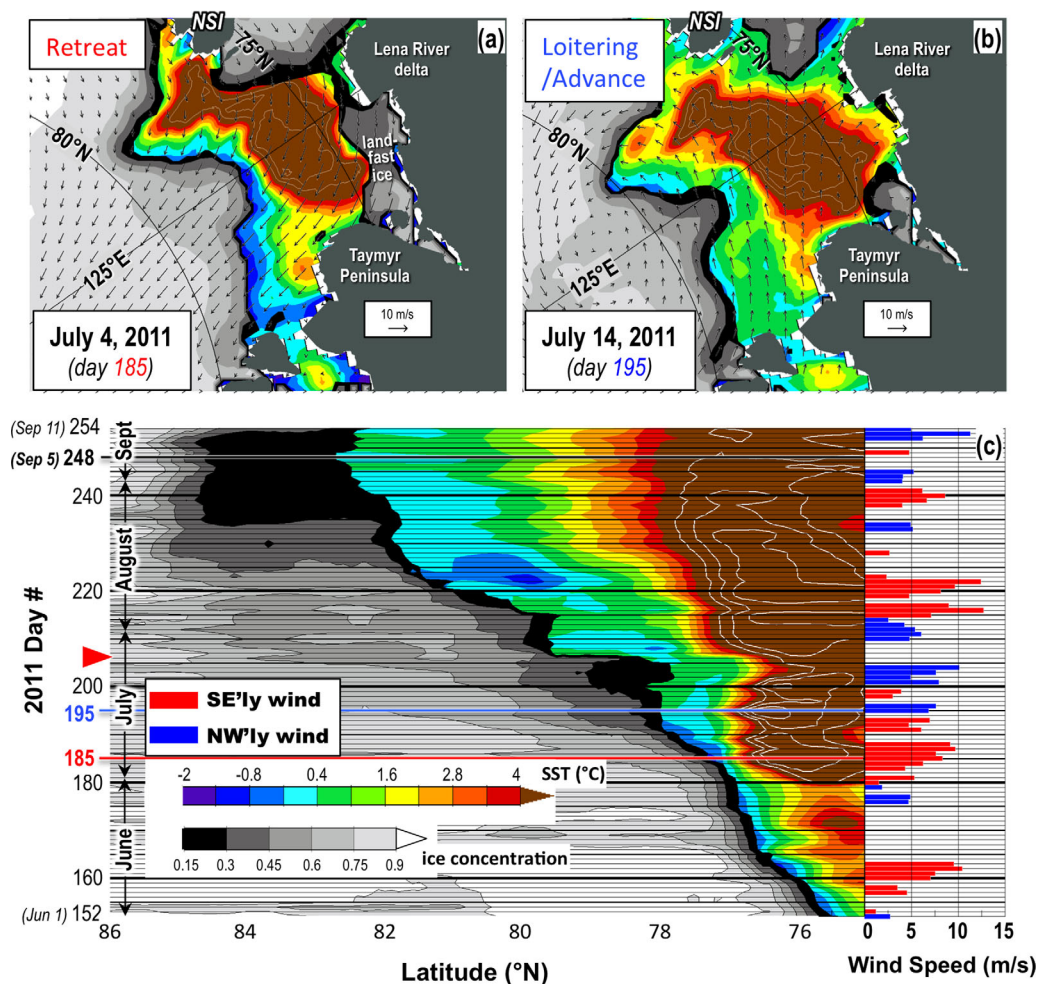
Figure 12. Conditions in the Laptev Sea on (a) 4 July 2011 during ice retreat over much of the domain, and on (b) 14 July 2011 during ice loitering/advance in the western part of the domain. Shown are ice concentration (gray contours), open water SST (color contours with additional white contours for 6°C, 7°C, and 8°C), and surface wind vectors (arrows). (c) Daily mean ice concentration and SST variation along longitude 125°E (marked in the top plots) over the retreat season, with SE'ly or NW'ly winds (in "ice north" coordinates, section 3.2) on the right. Also marked are Days 185 and 195 from Figures 12a and 12b. The red triangle marks Day 206, discussed in the text.

the winds are southeasterly (SE'ly) and thus "retreat favorable" or northwesterly (NW'ly) and "advance/loitering favorable." This is just a rough indicator of the forcing that may cause these ice edge displacements; a more detailed analysis is presented below.

A sample day from 2011 with strong retreat is shown in Figure 12a, with south/southeasterly winds along the ice edge (except in the far eastern part of the domain). As the ice edge was pushed northward by the wind, it compacted (note the closely spaced ice concentration contours) and left in its wake cold SSTs that were until recently ice covered. Figure 12b shows the situation ten days later, when a relatively small-scale cyclone was centered just north of the ice edge. This cyclone generated west/northwest winds along the ice edge in the western 2/3 of the domain that caused loitering and in some locations, advance of the ice edge. We also note that the ice edge was wider over this area than in Figure 12a, and SSTs near the ice edge were warmer.

Figure 12c provides a Hovmöller diagram of ice concentration and SST as functions of meridional distance along 125°E and day of the 2011 retreat season. Also shown is the daily surface wind speed, marked as SE'ly (i.e., retreat-favorable) or NW'ly (i.e., advance/loitering-favorable). Generally, the ice and ocean responses to surface winds noted in Figures 12a and 12b hold for the entire retreat season. Sea ice retreats strongly in response to SE'ly winds (e.g., mid-June, early July, and early August), leaving cool SSTs near the ice edge. On
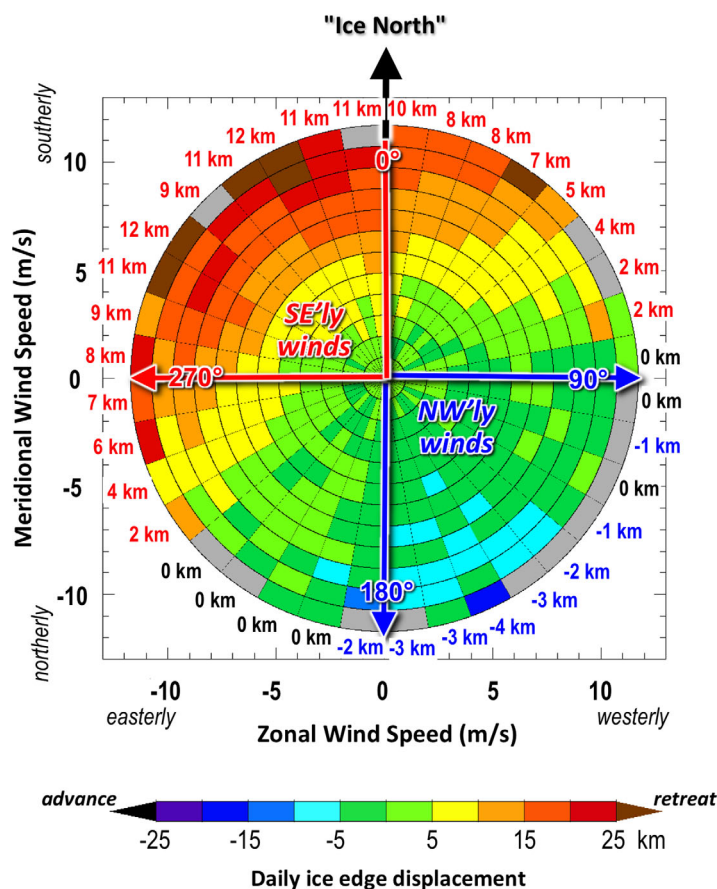
Figure 13. Daily ice edge displacement (colored boxes) as a function of wind speed and direction (axes), relative to "ice north" at the top. Gray boxes denote bins with fewer than 10 observations. Observations are every 25 km along all ice edges for every day of the retreat season in the Laptev Sea over the years 2007–2013, not including areas within 100 km of coastlines (Figure 10a). Also shown around the perimeter are 10° radial means of ice edge displacement (red for retreat, blue for advance). The red arrows delimit the southeasterly (SE'ly) quadrant over which winds are retreat favorable, while the blue arrows delimit the northwesterly (NW'ly) quadrant over which winds are advance or loitering favorable.

the other hand, NW'ly winds (e.g., mid/late July) are generally associated with loitering or weak advance of the ice edge, and slightly warmer near-ice SSTs. Note that the strong retreat during late July (Days 205–207, red triangle) was not associated with strong wind forcing. Instead, this resulted from an ice edge protuberance (see Figure 12b) which retreated zonally away from 125°E, i.e., there was significant two-dimensional motion of the ice edge at this time that is not captured in the Hovmöller diagram.

To account for interannual variability in this area, which can be large (Figure 2) [e.g., *Haas and Eicken*, 2001], we now turn to a broader analysis of ice edge motion in the Laptev Sea, by analyzing ice, wind, and ocean statistics at the ice edge over the 7 years 2007–2013. To start, Figure 13 provides a more complete analysis (relative to Figure 11d) of ice displacement in response to surface wind forcing. Ice advance is generally quite weak in the loitering-prone Laptev Sea, and is mostly forced by northwesterly winds. On the other hand, ice retreat is associated with a broader range

of wind directions, most strongly southeasterly, but also extending into the southwesterly and northeasterly quadrants. This is likely influenced by thermodynamic forcing, i.e., melting, which during the summer enhances retreat independently of the wind forcing.
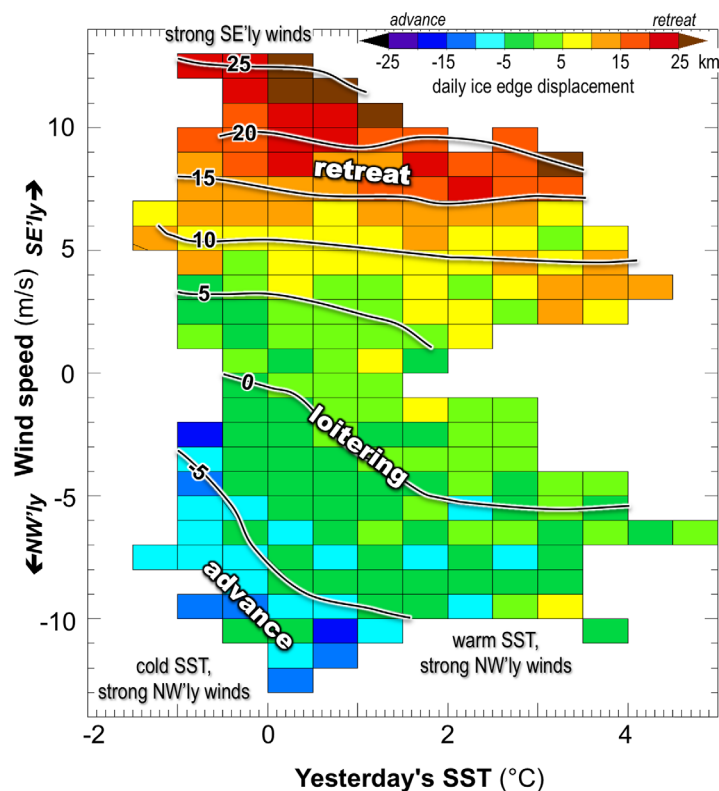
The surface wind angle associated with the strongest advance is ~30° counterclockwise or "to the left" of pure advance, while the angles for strongest retreat lie within the range 30°–60° to the left of pure retreat. This is similar to the 29° angle that individual ice floes move in response to surface winds [*Overland et al.*, 1984], although with more turning for retreat. Light winds tend to induce weak ice edge displacements, or loitering, as do west/southwesterly and north/northeasterly winds.

We now return to the effect of SST on ice displacement. Figure 12c is illustrative, but it only follows ice concentration and SST evolution along a single longitude for a single retreat season. A more complete analysis is presented in Figure 14, which shows how SST near the Laptev Sea ice edge affects the relationship between near-surface wind forcing and the resulting ice edge motion, using statistics from 2007 to 2013 along all ice edges. We here use the mean open water SST within 100 km of the ice edge, recognizing the long (~150 km) length scale smoothing in this data set [*Reynolds et al.*, 2007].

To first order, we see similar behavior to that shown in Figure 13, i.e., stronger winds tend to produce stronger retreat or advance. So how does SST affect ice edge displacement? The generally horizontal contours in the upper half of Figure 14 imply that it has little effect on retreat, although there is some influence at the

Figure 14. Ice edge displacement (km, colored pixels and black contours) from the previous day to the present day, as a function of (i) open water SST within 100 km of the ice edge from the previous day, and (ii) surface wind speed in SE'ly or NW'ly directions (in "ice north" coordinates, section 3.2) averaged over the previous and present days. Observations are every 25 km along all ice edges for every day of the retreat season in the Laptev Sea over the years 2007–2013. Pixels with fewer than 10 observations are not plotted.

warmest SSTs. On the other hand, ice advance is strongly influenced by SST; i.e., advance beyond our loitering threshold of 8 km/d (section 3) only occurs for the coldest SSTs. This makes intuitive sense: Under NW'ly wind forcing, the ice edge loiters if the water is warm enough to melt ice floes as fast as the wind can push them into the open water (on daily mean time scales). That is, when the wind pushes ice toward the warm open water, individual floes move into this water and melt, but the ice edge itself appears to be stationary (i.e., it loiters).

The linear relationship between surface wind forcing and the resulting sea ice edge displacement is presented in Figure 15a. This plot draws its data from the bins in Figure 14 that lie to the left of the SST = 1°C mark. Figure 15a shows that for cold temperatures, a significant linear relationship exists between wind forcing and both retreat

and advance. A corresponding plot for SSTs warmer than 1°C (not shown) indicates that a similar relationship holds for retreat, but no statistically significant linear fit can be found for advance.

We can also turn this relationship around and ask, How does ice retreat affect open water SSTs near the ice edge? This was explored qualitatively in Figure 12, where we saw that strong retreat exposed previously ice-covered ocean and thus left cold water in its wake during 2011 along 125°E. A more complete analysis for all ice edges in the Laptev region over 2007–2013 is presented in Figure 15b, which confirms that stronger ice edge retreat leads to colder open water SSTs.
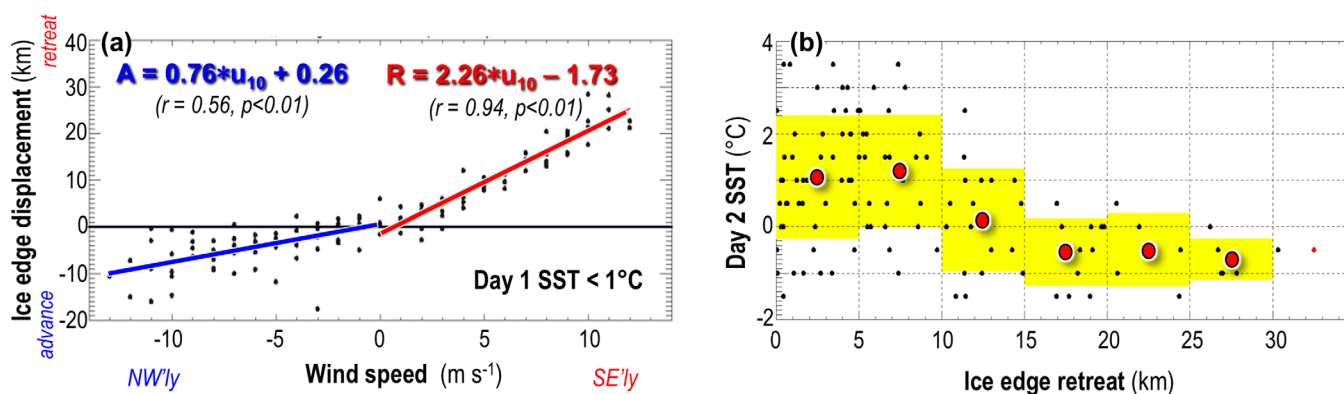
5.4. Wind and SST: A Simple Heat Flux Calculation

Figures 14 and 15 indicate that when relatively warm water resides near the ice edge, a NW'ly wind tends to induce loitering rather than southward advance of the ice edge. Loitering thus involves two processes: (i) advection of ice floes from the pack into the warm open water, and (ii) melting of these floes. Melting starts as soon as the floes enter the warm water, and will persist to some extent even if the wind moderates and/or veers. The question then becomes, are the observed SSTs really warm enough to cause loitering on the daily time scales we have considered here? We answer this in two ways. First, the analysis presented previously clearly shows the presence of loitering in the SIZ and at the winter ice extent maximum. The latter is an area well known for semistationary ice edges that have been traditionally linked to warm waters from the south [e.g., *Arthun et al.*, 2012; *Li et al.*, 2014].

Second, we present a simple calculation of heat fluxes that provides an estimate of how much ice can melt in one day. The ice thickness change Δh_i over a time period Δt forced by an ocean that is above its freezing point by an amount ΔT is provided by:

Figure 15. (a) Ice edge displacement from Day 1 to Day 2, as a function of surface wind speed averaged over the 2 days. Each black dot is a pixel value from Figure 14, but only for near-edge sea surface temperatures (SSTs) on Day 1 that are less than 1°C. Also shown are separate linear fits to NW'ly (blue line) and SE'ly (red line) wind forcing. (b) Day 2 SST as a function of ice edge retreat between Day 1 and Day 2 (black dots). Also shown are mean SSTs for 5 km retreat bins (red dots) and ± 1 standard deviation (yellow rectangles).

$$\rho_w c_p c_h u_* \Delta T = \rho_i L_i \Delta h_i / \Delta t, \tag{1}$$

where $\rho_w = 1025$ kg m^{-3} and $\rho_i = 900$ kg m^{-3} are the densities of seawater and sea ice, $c_p = 4200$ J kg^{-1} °C^{-1} is the heat capacity of seawater at constant pressure, $c_h = 0.01$ is a dimensionless heat transfer coefficient for melting sea ice at the freezing point [*Notz et al.*, 2003], $u_* = 0.01$ m s^{-1} is a typical friction velocity (proportional to the ice-ocean stress), $L_i = 3 \times 10^5$ J kg^{-1} is the latent heat of fusion of sea ice, and $\Delta t = 1$ day. For $\Delta T = 2.6$°C (about the middle of loitering values in Figure 14, given a freezing point of about -1.6°C), equation (1) provides an estimate of daily ice thickness loss $\Delta h_i = 36$ cm. This does not account for lateral melting, which could be substantial for the smaller floes often found at the ice edge [*Steele*, 1992]. This amount of melt is roughly equal to the ice thickness at the outer edge of the summer ice pack [*Laxon et al.*, 2013], thus supporting our hypothesized SST-based loitering mechanism.

Two advective processes might act to slow this melting process. First, NW'ly winds originate over the ice pack and are thus likely cooler than the warm open water over which they force ice floes. In the summer, we estimate that this will cool SSTs by only ~ 0.05–0.1°C/d (assuming an air-sea temperature difference of 2°C, surface wind of 5–10 m s^{-1}, and mixed layer depth of 5 m). The effect could be larger, up to ~ 0.5°C/d, in spring (assuming an air-sea temperature difference of 20°C, a strong surface wind of 10 m s^{-1}, and a thicker mixed layer of 10 m). Second, one might imagine that some cold surface water might also travel with the ice floes into the warm open water. However, ice is much more mobile in response to wind forcing relative to even a thin ocean surface layer, e.g., the mass of a 0.5 m thick ice floe is less than one tenth that of a 5 m thick ocean surface layer. Thus while advection of cold air and/or cold water will act to slow ice melting under NW'ly wind forcing (and may be dominant in extreme cases), we find that melting usually prevails and causes loitering.

5.5. Wind and SST: The Big Picture

Loitering happens at the winter ice edge every year, where the expanding ice pack during the fall meets large-scale ocean surface thermal fronts and then ceases (or dramatically slows) its further expansion. This is a well-known phenomenon. The new aspect discussed here is the replication of similar physics within the SIZ to the north of the winter extent maximum. How does this happen?

The key factor that induces loitering is the presence of warm SSTs near the ice edge, assuming that wind forcing is random and thus generates loitering-favorable winds on synoptic time scales. One way this can occur within the SIZ is to have the retreating ice edge "chased" by warm ocean currents where these are strong. An example is the Barents and Kara Seas, where inflowing warm Atlantic Water moves north/northeastward with the retreating ice edge, generating frequent loitering (Figures (2 and 6), and 7). A similar effect (although with smaller amplitude) is forced by Pacific Water currents in the Bering and Okhotsk Seas and, to a lesser extent, in the Chukchi Sea [*Brugler et al.*, 2014].

What if there are no strong ocean currents to warm the ocean near the ice edge? In this case, the main heat source is likely solar radiative forcing, which warms the ocean in spring and summer in response to sea ice
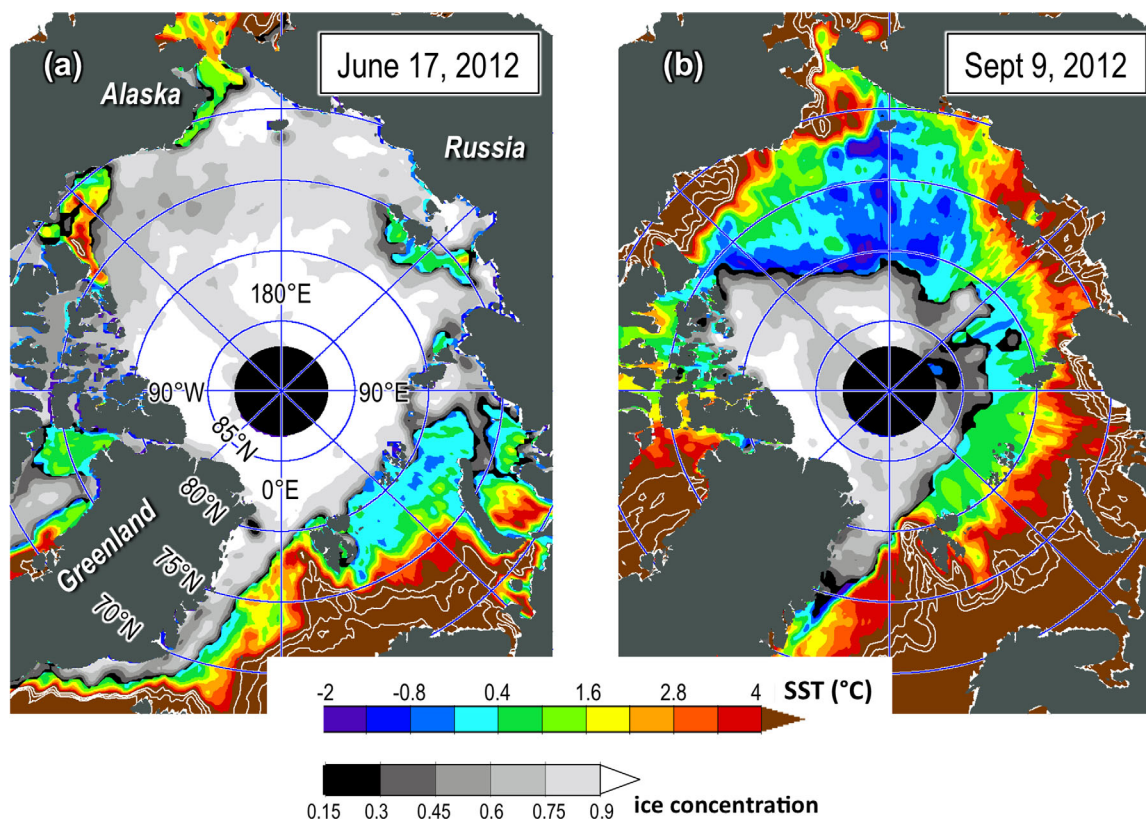
Figure 16. Sea surface temperature (color) and sea ice concentration (gray scale) on 2 days in 2012. As in Figure 12, extra temperature contours (white) are provided for 5°C, 6°C, and 7°C.

retreat [*Steele et al.*, 2010]. This process is strongest where ice retreat is early enough to expose open water before (or not too long after) the radiative maximum at summer solstice.

Figure 16a shows an example of ice coverage and SSTs in mid-June 2012. At this time, the retreating ice edge has just recently entered the Arctic Ocean after the RA hiatus (Figure 1). Warm water is following the ice edge northward in the Barents, Kara, and Chukchi Seas, likely forced by a combination of ocean current advection and additional heat input from atmospheric (largely, solar radiative) fluxes. Also evident in this figure are several areas of geographically isolated ice retreat and warm SSTs. One such area is the eastern Beaufort Sea, where strong spring easterly winds tend to force early ice retreat [*Steele et al.*, 2015], allowing solar forcing to warm the upper ocean. A second area of early ice retreat and warm SSTs is the Laptev Sea north of the coastal landfast ice zone, as discussed in section 5.3. A third area is in northern Baffin Bay, likely forced by solar warming of an area that was at least partly open during the ice growth season as the North Water polynya [e.g., *Ingram et al.*, 2002].

Conversely, sea ice tends to linger later into the retreat season in some peripheral seas, i.e., the western Beaufort and East Siberian Seas, as well as the Arctic Ocean areas adjacent to most of the Canadian Arctic Archipelago (CAA). In fact, the thick ice near the CAA never substantially melts out during the retreat season. Ice usually does retreat in the western Beaufort Sea, although later in the season because it is generally thicker than that in the east [*Steele et al.*, 2015]. The cause of late retreat in the East Siberian Sea ice is perhaps less clear, although it is likely linked to thick ice during years with a large Beaufort Gyre [*Stroeve et al.*, 2011].

In any case, areas with late retreat expose the ocean surface to the atmosphere at a time well past the summer solstice, when solar warming is weak [*Lindsay*, 1998; *Serreze et al.*, 2007]. This produces only weak SST warming, and thus minimal loitering. This is also a likely explanation for the minimal loitering seen in the northern Amerasian Basin SIZ during 2012 (Figures 2 and 6), which occurred during ice retreat in August and early September [*Parkinson and Comiso*, 2013], when the air-sea energy balance was close to zero and

thus warming of the recently exposed ocean was small (Figure 16b). Generally speaking, recent years with enhanced ice retreat (Figure 1) and an expanding SIZ (Figure 9a) have experienced late-season exposure of open water to the atmosphere, which induces only minimal ocean warming via downward shortwave fluxes, and thus negligible change in the absolute area of loitering (Figure 9a). The key point here is that loitering is intimately tied to the timing of sea ice retreat: early retreat tends to induce loitering, while late retreat does not.

6. Summary and Discussion

Ice edge loitering is a phenomenon in which the summertime retreat of the ice edge slows, or "loiters," most commonly for several days and up to ∼1.5 weeks (Figure 8c). We find that this is more likely to happen in some locations than in others (Figure 7). Loitering occupies about 20–25% of the Seasonal Ice Zone (SIZ) area (Figure 8a) and generally occurs in any one location during the retreat season 1–3 times (Figure 8b), separated by intervals of a few days or at times, a few weeks (Figure 8d).

Loitering is mainly caused by winds that blow sea ice toward warm open water, where individual floes melt. On the daily time scales considered here, this creates an apparently stationary ice edge, even though ice floe displacement is in fact happening. This mechanism explains why the Eastern Beaufort Sea, Northern Chukchi Sea, Laptev Sea, and Northern Baffin Bay are "loitering-prone" areas (Figure 7), since these areas tend to open early in the retreat season and thus warm via atmospheric heating. It also explains why the generally late-opening East Siberian and Western Beaufort Seas are relatively loitering free. We find that some advance of the ice edge can in fact happen during the retreat season when SSTs near the ice edge are cool (Figures 14 and 15).

Perhaps surprisingly, the absolute area of loitering within the SIZ has not changed substantially over the past 25 years, even as the SIZ itself has grown in response to dramatic summertime ice loss (Figure 9). The reason is that recent SIZ expansion has mostly happened late in the retreat season, when atmospheric warming of the ocean surface is weak. A prime example is the lack of loitering seen in the northern Amerasian Basin SIZ during 2012 (Figures 2b, 6e, and 16b). Will this change in the future? It might, if the seasonal timing of major ice retreat within the Arctic Ocean shifts toward earlier months. In this case, retreat would allow more atmospheric warming of the newly exposed ocean surface, which as we have seen is the main cause of loitering.

We have found loitering in two-observational data sets that use satellite passive microwave ice concentration data (SSMIS, AMSR2), as well as a multisensor satellite and in situ merged product (MASIE). These products do contain errors that affect their estimate of daily ice edge position and motion. Our confidence that loitering is "real" is bolstered by its presence in all of these products, and by its correlation with SST and wind that provides a reasonable physical mechanism to explain the phenomenon. Nonetheless, we acknowledge a need for further confirmation of ice edge loitering, perhaps by high-resolution visible imagery during rare periods of consecutive cloud-free days, or by coastal radars, autonomous unmanned vehicles, high-resolution numerical models, or other methods.

What are the physical and biological implications of ice edge loitering? Imagine an ice edge that retreats at a constant (or slowly evolving) rate throughout the entire season. In this case, the physical air/sea/ice conditions at the edge remain generally constant on monthly time scales, simply advecting northward with the general retreat. Now imagine an ice edge that is instead retreating at a highly nonconstant rate, i.e., loitering for up to a week, then suddenly moving quickly northward in response to a shift in the wind forcing. A loitering edge will melt in place for days, thus enhancing surface stratification (which will in turn affect ocean surface warming), modifying the floe diameter distribution toward smaller floes, and affecting the atmospheric boundary layer via its response to surface warming and ice pack changes. This will likely have profound implications for the ice edge ecosystem, as enhanced stratification retains plankton near the surface but suppresses nutrient upwelling. When the wind shifts and the ice edge moves quickly away from this loitering location, how does the formerly stratified ocean and ecosystem that has been left behind evolve over time? What are the new conditions at the now rapidly moving ice edge? What happens if the ice edge returns to its original location and experiences another loitering event? These and other topics regarding ice edge loitering remain subjects for future research.

References

Arthun, M., T. Eldevik, L. H. Smedsrud, O. Skagseth, and R. B. Ingvaldsen (2012), Quantifying the influence of Atlantic heat on Barents Sea Ice variability and retreat, *J. Clim.*, *25*(13), 4736–4743, doi:10.1175/JCLI-D-11-00466.1.

Beitsch, A., L. Kaleschke, and S. Kern (2014), Investigating high-resolution AMSR2 sea ice concentrations during the February 2013 fracture event in the Beaufort Sea, *Remote Sens.*, *6*(5), 3841–3856, doi:10.3390/rs6053841.

Brugler, E. T., R. S. Pickart, G. W. K. Moore, S. Roberts, T. J. Weingartner, and H. Statscewich (2014), Seasonal to interannual variability of the Pacific water boundary current in the Beaufort Sea, *Prog. Oceanogr.*, *127*, 1–20, doi:10.1016/j.pocean.2014.05.002.

Cavalieri, D. J., and C. L. Parkinson (2012), Arctic sea ice variability and trends, 1979–2010, *Cryosphere*, *6*(4), 881–889, doi:10.5194/tc-6-881-2012.

Cavalieri, D. J., et al. (1992), NASA sea ice validation program for the DMSP SSM/I: Final report, *NASA Tech. Memo. 104559*, 126 pp., NASA, Washington, D. C.

Cavalieri, D. J., C. L. Parkinson, P. Gloersen, and H. Zwally (1996), *Sea Ice Concentrations From Nimbus-7 SSMR and DMSP SSM/I-SSMIS Passive Microwave Data*, NASA DAAC at the Natl. Snow and Ice Data Cent., Boulder, Colo. [Updated yearly.]

Eicken, H., I. Dmitrenko, K. Tyshko, A. Darovskikh, W. Dierking, U. Blahak, J. Groves, and H. Kassens (2005), Zonation of the Laptev Sea land-fast ice cover and its importance in a frozen estuary, *Global Planet. Change*, *48*(1–3), 55–83, doi:10.1016/j.gloplacha.2004.12.005.

Eisenman, I. (2010), Geographic muting of changes in the Arctic sea ice cover, *Geophys. Res. Lett.*, *37*, L07701, doi:10.1029/2010GL043741.

Fetterer, F., M. Savoie, S. Helfrich, and P. Clemente-Colon (2010), *Multisensor Analyzed Sea Ice Extent—Northern Hemisphere*, Natl. Snow and Ice Data Cent., Boulder, Colo., doi:10.7265/N5GT5K3K.

Haas, C., and H. Eicken (2001), Interannual variability of summer sea ice thickness in the Siberian and central Arctic under different atmospheric circulation regimes, *J. Geophys. Res.*, *106*(C3), 4449–4462.

Ingram, R. G., J. Bacle, D. G. Barber, Y. Gratton, and H. Melling (2002), An overview of physical processes in the North Water, *Deep Sea Res., Part II*, *49*(22–23), 4893–4906.

Kwok, R., A. Schweiger, D. A. Rothrock, S. Pang, and C. Kottmeier (1998), Sea ice motion from satellite passive microwave imagery assessed with ERS SAR and buoy motions, *J. Geophys. Res.*, *103*(C4), 8191–8214.

Laxon, S. W., et al. (2013), CryoSat-2 estimates of Arctic sea ice thickness and volume, *Geophys. Res. Lett.*, *40*, 732–737, doi:10.1002/grl.50193.

Li, L. H., A. J. Miller, J. L. McClean, I. Eisenman, and M. C. Hendershott (2014), Processes driving sea ice variability in the Bering Sea in an eddying ocean/sea ice model: Anomalies from the mean seasonal cycle, *Ocean Dyn.*, *64*(12), 1693–1717, doi:10.1007/s10236-014-0769-7.

Lindsay, R. W. (1998), Temporal variability of the energy balance of thick Arctic pack ice, *J. Clim.*, *11*(3), 313–333.

Lindsay, T., M. Wensnahan, A. Schweiger, and J. Zhang (2014), Evaluation of seven different atmospheric reanalysis products in the Arctic, *J. Clim.*, *27*(7), 2588–2606, doi:10.1175/JCLI-D-13-00014.1.

Lott, J. N. (2004), The quality control of the Integrated Surface Hourly databaseextended abstract, paper presented at 14th Conference on Applied Climatology, Seattle, Wash.

Martin, S., and R. Drucker (1997), The effect of possible Taylor columns on the summer ice retreat in the Chukchi Sea, *J. Geophys. Res.*, *102*(C5), 10,473–10,482, doi:10.1029/97JC00145.

Martin, T., and R. Gerdes (2007), Sea ice drift variability in Arctic Ocean Model Intercomparison Project models and observations, *J. Geophys. Res.*, *112*, C04S10, doi:10.1029/2006JC003617.

Nghiem, S. V., P. Clemente-Colon, I. G. Rigor, D. K. Hall, and G. Neumann (2012), Seafloor control on sea ice, *Deep Sea Res., Part II*, *77–80*, 52–61, doi:10.1016/j.dsr2.2012.04.004.

Notz, D., M. G. McPhee, M. G. Worster, G. A. Maykut, K. H. Schlunzen, and H. Eicken (2003), Impact of underwater-ice evolution on Arctic summer sea ice, *J. Geophys. Res.*, *108*(C7), 3223, doi:10.1029/2001JC001173.

Olason, E., and D. Notz (2014), Drivers of variability in Arctic sea-ice drift speed, *J. Geophys. Res. Oceans*, *119*, 5755–5775, doi:10.1002/2014JC009897.

Overland, J. E., H. O. Mofjeld, and C. H. Pease (1984), Wind-driven ice drift in a shallow sea, *J. Geophys. Res.*, *89*(C4), 6525–6531, doi:10.1029/JC089iC04p06525.

Parkinson, C. L., and D. J. Cavalieri (2008), Arctic sea ice variability and trends, 1979–2006, *J. Geophys. Res.*, *113*, C07003, doi:10.1029/2007JC004558.

Parkinson, C. L., and J. C. Comiso (2013), On the 2012 record low Arctic sea ice cover: Combined impact of preconditioning and an August storm, *Geophys. Res. Lett.*, *40*, 1356–1361, doi:10.1002/grl.50349.

Rampal, P., J. Weiss, and D. Marsan (2009), Positive trend in the mean speed and deformation rate of Arctic sea ice, 1979–2007, *J. Geophys. Res.*, *114*, C05013, doi:10.1029/2008JC005066.

Reynolds, R. W., N. A. Rayner, T. M. Smith, D. C. Stokes, and W. Q. Wang (2002), An improved in situ and satellite SST analysis for climate, *J. Clim.*, *15*(13), 1609–1625.

Reynolds, R. W., T. M. Smith, C. Liu, D. B. Chelton, K. S. Casey, and M. G. Schlax (2007), Daily high-resolution-blended analyses for sea surface temperature, *J. Clim.*, *20*(22), 5473–5496.

Rothrock, D. A., and A. S. Thorndike (1984), Measuring the sea ice-floe size distribution, *J. Geophys. Res.*, *89*(C4), 6477–6486.

Schweiger, A., R. Lindsay, J. L. Zhang, M. Steele, H. Stern, and R. Kwok (2011), Uncertainty in modeled Arctic sea ice volume, *J. Geophys. Res.*, *116*, C00D06, doi:10.1029/2011JC007084.

Serreze, M. C., A. P. Barrett, A. G. Slater, M. Steele, J. L. Zhang, and K. E. Trenberth (2007), The large-scale energy budget of the Arctic, *J. Geophys. Res.*, *112*, D11122, doi:10.1029/2006JD008230.

Spreen, G., L. Kaleschke, and G. Heygster (2008), Sea ice remote sensing using AMSR-E 89-GHz channels, *J. Geophys. Res.*, *113*, C02S03, doi:10.1029/2005JC003384.

Spreen, G., R. Kwok, and D. Menemenlis (2011), Trends in Arctic sea ice drift and role of wind forcing: 1992–2009, *Geophys. Res. Lett.*, *38*, L19501, doi:10.1029/2011GL048970.

Steele, M. (1992), Sea ice melting and floe geometry in a simple ice-ocean model, *J. Geophys. Res.*, *97*(C11), 17,729–17,738.

Steele, M., R. Morley, and W. Ermold (2001), PHC: A global ocean hydrography with a high-quality Arctic Ocean, *J. Clim.*, *14*(9), 2079–2087.

Steele, M., W. Ermold, and J. L. Zhang (2008), Arctic Ocean surface warming trends over the past 100 years, *Geophys. Res. Lett.*, *35*, L02614, doi:10.1029/2007GL031651.

Steele, M., J. Zhang, and W. Ermold (2010), Mechanisms of summertime upper Arctic Ocean warming and the effect on sea ice melt, *J. Geophys. Res.*, *115*, C11004, doi:10.1029/2009JC005849.

Steele, M., S. Dickinson, J. L. Zhang, and R. W. Lindsay (2015), Seasonal ice loss in the Beaufort Sea: Toward synchrony and prediction, *J. Geophys. Res. Oceans*, *120*, 1118–1132, doi:10.1002/2014JC010247.

Stroeve, J. C., J. Maslanik, M. C. Serreze, I. Rigor, W. Meier, and C. Fowler (2011), Sea ice response to an extreme negative phase of the Arctic Oscillation during winter 2009/2010, *Geophys. Res. Lett.*, *38*, L02502, doi:10.1029/2010GL045662.

Tivy, A., S. E. L. Howell, B. Alt, S. McCourt, R. Chagnon, G. Crocker, T. Carrieres, and J. J. Yackel (2011), Trends and variability in summer sea ice cover in the Canadian Arctic based on the Canadian Ice Service Digital Archive, 1960–2008 and 1968–2008, *J. Geophys. Res.*, *116*, C06027, doi:10.1029/2011JC007248.

van der Hoven, I. (1957), Power spectrum of horizontal wind speed in the grequency range from 0.0007 to 900 cycles per hour, *J. Meteorol.*, *14*, 160–164.